


Article

# On the Hydration of Heavy Rare Earth Ions: $\text{Ho}^{3+}$ , $\text{Er}^{3+}$ , $\text{Tm}^{3+}$ , $\text{Yb}^{3+}$ and $\text{Lu}^{3+}$ —A Raman Study

 Wolfram Rudolph <sup>1,\*</sup>  and Gert Irmer <sup>2</sup>
<sup>1</sup> TU Dresden, Medizinische Fakultät, Institut für Virologie im MTZ, Fiedlerstr. 42, 01307 Dresden, Germany

<sup>2</sup> Technische Universität Bergakademie Freiberg, Institut für Theoretische Physik, Leipziger Str. 23, 09596 Freiberg, Germany; irmer@physik.tu-freiberg.de

\* Correspondence: Wolfram.Rudolph@tu-dresden.de; Tel.: +49-0351-458-6200

Academic Editor: Keith C. Gordon

Received: 3 April 2019; Accepted: 20 May 2019; Published: 21 May 2019



**Abstract:** Raman spectra of aqueous  $\text{Ho}^{3+}$ ,  $\text{Er}^{3+}$ ,  $\text{Tm}^{3+}$ ,  $\text{Yb}^{3+}$ , and  $\text{Lu}^{3+}$ -perchlorate solutions were measured over a large wavenumber range from 50–4180  $\text{cm}^{-1}$ . In the low wavenumber range (terahertz region), strongly polarized Raman bands were detected at 387  $\text{cm}^{-1}$ , 389  $\text{cm}^{-1}$ , 391  $\text{cm}^{-1}$ , 394  $\text{cm}^{-1}$ , and 396  $\text{cm}^{-1}$ , respectively, which are fairly broad (full widths at half height at  $\sim 52 \text{ cm}^{-1}$ ). These isotropic Raman bands were assigned to the breathing modes,  $\nu_1 \text{ Ln-O}$  of the heavy rare earth (HRE) octaaqua ions,  $[\text{Ln}(\text{H}_2\text{O})_8]^{3+}$ . The strong polarization of these bands (depolarization degree  $\sim 0$ ) reveals their totally symmetric character. The vibrational isotope effect was measured in  $\text{Yb}(\text{ClO}_4)_3$  solutions in  $\text{H}_2\text{O}$  and  $\text{D}_2\text{O}$  and the shift of the  $\nu_1$  mode in changing from  $\text{H}_2\text{O}$  to  $\text{D}_2\text{O}$  further supports the character of the band. The  $\text{Ln-O}$  bond distances of these HRE ions ( $\text{Ho}^{3+}$ ,  $\text{Er}^{3+}$ ,  $\text{Tm}^{3+}$ ,  $\text{Yb}^{3+}$ , and  $\text{Lu}^{3+}$ ) follow the order of  $\text{Ho-O} > \text{Er-O} > \text{Tm-O} > \text{Yb-O} > \text{Lu-O}$  which correlates inversely with the band positions of the breathing modes of their corresponding octaaqua ions  $[\text{Ln}(\text{OH}_2)_8]^{3+}$ . Furthermore, the force constants,  $k_{\text{Ln-O}}$ , were calculated for these symmetric stretching modes. Ytterbium perchlorate solutions were measured over a broad concentration range, from 0.240  $\text{mol}\cdot\text{L}^{-1}$  to 2.423  $\text{mol}\cdot\text{L}^{-1}$ , and it was shown that with increasing solute concentration outer-sphere ion pairs and contact ion pairs were formed. At the dilute solution state ( $\sim 0.3 \text{ mol}\cdot\text{L}^{-1}$ ), the fully hydrated ions  $[\text{Yb}(\text{H}_2\text{O})_8]^{3+}$  exist, while at higher concentrations ( $C_T > 2 \text{ mol}\cdot\text{L}^{-1}$ ), ion pairs are formed. The concentration behavior of  $\text{Yb}(\text{ClO}_4)_3$  (aq) shows similar behavior to the one observed for  $\text{La}(\text{ClO}_4)_3$ (aq),  $\text{Ce}(\text{ClO}_4)_3$ (aq) and  $\text{Lu}(\text{ClO}_4)_3$ (aq) solutions. In ytterbium chloride solutions in water and heavy water, representative for the behavior of the other HRE ions, 1:1 chloro-complex formation was detected over the concentration range from 0.422–3.224  $\text{mol}\cdot\text{L}^{-1}$ . The 1:1 chloro-complex in  $\text{YbCl}_3$ (aq) is very weak, diminishing rapidly with dilution and vanishing at a concentration  $< 0.4 \text{ mol}\cdot\text{L}^{-1}$ .

**Keywords:** Raman spectroscopy; aqueous  $\text{Lu}(\text{ClO}_4)_3$ -,  $\text{Yb}(\text{ClO}_4)_3$ -,  $\text{Tm}(\text{ClO}_4)_3$ -,  $\text{Er}(\text{ClO}_4)_3$ - and  $\text{Ho}(\text{ClO}_4)_3$ - solutions;  $\text{YbCl}_3$ -solutions;  $\nu_1 \text{ Ln-O}$  breathing modes;  $\text{Yb}^{3+}$ - chloro-complex species

## 1. Introduction

In aqueous solution, the HRE ions of holmium, erbium, thulium, ytterbium, and lutetium exist in the trivalent state [1] and, with their high charge to radius ratio, are strongly hydrated [2,3]. The HRE ions possess eight water molecules arranged in a square antiprismatic geometry ( $S_8$  symmetry) in their first coordination sphere. The hydration geometry of heavy rare earth ions in aqueous solution was determined by X-ray (XRD) and neutron diffraction (ND) [4–6] as well as extended X-ray absorption fine structure (EXAFS) [7–10] techniques. Computer simulations contributed to clarifying the details of the structure and dynamics of the waters in the first hydration sphere of the HRE ions [11–13] and their results confirmed the octahedral coordination.

While XRD and neutron diffraction measurements [4–6] are carried out in concentrated solutions, EXAFS spectra [7–10] are measured on dilute or moderately concentrated solutions. At high concentrations, however, it is known that the  $\text{Ln}^{3+}(\text{aq})$  ions form complex species/ion pairs with common ions ( $\text{Cl}^-$ ,  $\text{NO}_3^-$  and  $\text{SO}_4^{2-}$ ). Perchlorate, however, acts as a weak complex forming anion and the anion is therefore suitable for hydration studies.

Raman spectroscopy has been applied frequently to characterize hydrated metal ions and related species in aqueous solution and is especially useful in characterizing the species formed at the molecular level such as hydrated ions, ion pairs between metal ions and anions or metal ion hydrolysis. Raman measurements on aqueous  $\text{Ln}^{3+}(\text{aq})$  ions should allow, in principle, the characterization of the solution structure in greater detail. Recently, light rare earth solutions ( $\text{La}^{3+}$ ,  $\text{Ce}^{3+}$ ,  $\text{Pr}^{3+}$ ,  $\text{Nd}^{3+}$  and  $\text{Sm}^{3+}$ ) as well as the solution of the HRE ion,  $\text{Lu}^{3+}$ , have been measured using Raman spectroscopy [14–17] and it has been shown that the application of the so-called R-procedure is crucial in exploring the low frequency part of the Raman scattering.

The present study was undertaken to characterize the hydration and speciation in aqueous  $\text{Ho}^{3+}$ ,  $\text{Er}^{3+}$ ,  $\text{Tm}^{3+}$ , and  $\text{Yb}^{3+}$  perchlorate solutions.  $\text{Lu}^{3+}$ - solutions in water and heavy water have been measured and described in a recent publication [17] and these results are also included in this work. The  $\text{Ho}^{3+}$ -,  $\text{Er}^{3+}$ -,  $\text{Tm}^{3+}$ - and  $\text{Yb}^{3+}$ - perchlorate solutions were measured over broader concentration ranges and down to the terahertz frequency region at 22 °C. Furthermore,  $\text{Yb}(\text{ClO}_4)_3$  solutions in water and heavy water were measured in order to characterize the vibrational isotope effect changing from  $[\text{Yb}(\text{H}_2\text{O})_8]^{3+}$  to  $[\text{Yb}(\text{D}_2\text{O})_8]^{3+}$  and the symmetric stretching modes of the two species were observed.

In chloride solutions, however, it was shown that light rare earth ions form chloro-complex species, [14–17]. In order to clarify whether chloro-complex species may also form in these HRE chloride solutions,  $\text{YbCl}_3$  solutions were measured at varying concentrations in water and heavy water. Recently, inner-sphere chloro- complexes were detected in aqueous solutions on a variety of rare earth chloride solutions using Raman spectroscopy [14–17].

In this study, we are specifically interested in the vibrational characterization of the Ln–O stretching modes of the octahydrates (fully hydrated ions,  $[\text{Ln}(\text{OH}_2)_8]^{3+}$ ) in dilute perchlorate solutions. The formation of ion pairs between  $\text{Yb}^{3+}$  ions and perchlorate has been studied on a concentration series of  $\text{Yb}(\text{ClO}_4)_3$  solutions representative for other HRE ions. The influence of  $\text{Cl}^-$  on the fully hydrated  $\text{Ln}^{3+}(\text{aq})$  was studied exemplarily on  $\text{YbCl}_3$  solutions in water and heavy water. These results are discussed in connection with recently measured aqueous  $\text{LuCl}_3$  solutions [17].

## 2. Experimental Details and Data Analysis

### Preparation of Solutions

The rare earth ion concentrations of all solutions were analysed by complexometric titration [18]. The solution densities were determined pycnometrically at 22 °C and the molar ratios of water per salt calculated ( $R_w$ -values). The solution pH values were measured with pH meter S220 using a pH electrode InLab Expert Pro-ISM (Mettler –Toledo GmbH, Deutschland, Giessen). For Raman spectroscopic measurements, the solutions were filtered through a fine sintered glass frit (1–1.6  $\mu\text{m}$  pore size). The preparation of the lutetium perchlorate solutions at various concentrations were described earlier [17].

Ytterbium perchlorate solutions were prepared from  $\text{Yb}(\text{ClO}_4)_3 \cdot 6\text{H}_2\text{O}$  (Alfa-Aesar (Thermo Fisher), 99.9%, Kandel, Deutschland) dissolved with ultrapure water (PureLab Plus, Ultra-pure Water Purification Systems). A concentrated  $\text{Yb}(\text{ClO}_4)_3$  solution was prepared at  $2.423 \text{ mol}\cdot\text{L}^{-1}$  ( $R_w = 16.86$ ). This solution was acidified with a slight amount of  $\text{HClO}_4$  and a pH value at  $\sim 2.0$  was obtained. From this stock solution, the following dilution series was prepared:  $1.217 \text{ mol}\cdot\text{L}^{-1}$  ( $R_w = 39.30$ ),  $0.808 \text{ mol}\cdot\text{L}^{-1}$  ( $R_w = 62.13$ ),  $0.603 \text{ mol}\cdot\text{L}^{-1}$  ( $R_w = 85.16$ ) and  $0.240 \text{ mol}\cdot\text{L}^{-1}$  ( $R_w = 223.6$ ). The solutions were analysed for dissolved chloride with a 5%  $\text{AgNO}_3$  solution and the absence of a white  $\text{AgCl}$  precipitate was proof that the stock solution was free of Cl.

Two  $\text{Yb}(\text{ClO}_4)_3$  solutions in heavy water were prepared from a  $2.526 \text{ mol}\cdot\text{L}^{-1}$   $\text{Yb}(\text{ClO}_4)_3(\text{D}_2\text{O})$  stock solution with heavy water (99.9 atom% D; Sigma-Aldrich now Merck KGaA, Darmstadt, Germany) at  $1.276 \text{ mol}\cdot\text{L}^{-1}$  and  $0.779 \text{ mol}\cdot\text{L}^{-1}$ . The deuteration degree for the solution was determined at ~97% D.

$\text{YbCl}_3$  solutions were prepared from  $\text{YbCl}_3\cdot 6\text{H}_2\text{O}$  (Sigma-Aldrich, 99.5%) and ultrapure water (PureLab Plus, Ultra-pure Water Purification Systems, now ELGA Labwater, Celle, Deutschland) by weight at  $3.224 \text{ mol}\cdot\text{L}^{-1}$  ( $R_w = 15.64$ ),  $1.600 \text{ mol}\cdot\text{L}^{-1}$  ( $R_w = 33.06$ ),  $0.802 \text{ mol}\cdot\text{L}^{-1}$  ( $R_w = 67.55$ ) and  $0.400 \text{ mol}\cdot\text{L}^{-1}$  ( $R_w = 137$ ).

A  $3.300 \text{ mol}\cdot\text{L}^{-1}$   $\text{YbCl}_3$  stock solution in  $\text{D}_2\text{O}$  was used to prepare two dilute  $\text{YbCl}_3$  solutions with heavy water (99.9 atom% D; Sigma-Aldrich) at  $0.844 \text{ mol}\cdot\text{L}^{-1}$  and  $0.422 \text{ mol}\cdot\text{L}^{-1}$ . The deuteration degree in the dilute solutions was determined at ~96.5% D.

A  $\text{Tm}(\text{ClO}_4)_3$  solution was prepared from  $\text{Tm}_2\text{O}_3$  (Sigma-Aldrich, 99.9%) which was dissolved with  $6 \text{ mol}\cdot\text{L}^{-1}$   $\text{HClO}_4$  solution (Fisher Scientific GmbH, Schwerte, Deutschland) until a clear solution was obtained. The solute concentration was determined at  $1.897 \text{ mol}\cdot\text{L}^{-1}$  and two dilute solutions were prepared from the stock solution and triply distilled water by weight at  $0.980 \text{ mol}\cdot\text{L}^{-1}$  and  $0.315 \text{ mol}\cdot\text{L}^{-1}$ . These solutions contained a slight excess of  $\text{HClO}_4$ .

An  $\text{Er}(\text{ClO}_4)_3$  stock solution was a commercial product from Alfa-Aesar (Thermo Fisher) (Kandel, Deutschland) at 50 wt%, Reagent Grade (99.9%) at  $2.245 \text{ mol}\cdot\text{L}^{-1}$ . Two dilute solutions at  $1.123 \text{ mol}\cdot\text{L}^{-1}$  and at  $0.321 \text{ mol}\cdot\text{L}^{-1}$  were prepared by weight with ultrapure water. These solutions contained a slight excess of  $\text{HClO}_4$  (pH value ~1.5).

A  $\text{Ho}(\text{ClO}_4)_3$  stock solution was prepared from  $\text{Ho}_2\text{O}_3$  (Sigma-Aldrich, 99.9%) which was dissolved with  $6 \text{ mol}\cdot\text{L}^{-1}$   $\text{HClO}_4$  (Riedel-de Haen, 70 wt%) until a clear solution was obtained. The solute concentration was determined at  $1.675 \text{ mol}\cdot\text{L}^{-1}$ . Two dilute solutions at  $0.838 \text{ mol}\cdot\text{L}^{-1}$  and  $0.240 \text{ mol}\cdot\text{L}^{-1}$  were prepared by weight from the stock solution with ultrapure water. The solutions contained a slight excess of  $\text{HClO}_4$  (pH value ~1.75).

Raman spectroscopic measurements have been reported in detail elsewhere, so only a brief summary is given [19,20]. Raman spectra were measured in the macro chamber of the T 64000 Raman spectrometer from Jobin Yvon in a  $90^\circ$  scattering geometry at  $22^\circ\text{C}$ . A quartz cuvette was used (Hellma Analytics, Müllheim, Germany) with a 10 mm path length and a volume at  $1000 \mu\text{L}$ . The spectra were excited with the  $487.987 \text{ nm}$  or the  $514.532 \text{ nm}$  line of an  $\text{Ar}^+$  laser at a power level of  $1100 \text{ mW}$  at the sample. The  $\text{Yb}^{3+}$ -perchlorate and -chloride solutions have no visible absorption bands and therefore, both excitation wavelengths may be used.  $\text{Tm}(\text{ClO}_4)_3$  solutions were measured with the  $514.532 \text{ nm}$   $\text{Ar}^+$  line.  $\text{Er}(\text{ClO}_4)_3$  solutions were excited with the  $487.987 \text{ nm}$   $\text{Ar}^+$  line and only the most dilute solution could be measured reliably because the concentrated ones were strongly absorbing at the absorption gap at  $\sim 488 \text{ nm}$  of its UV-vis spectrum.  $\text{Ho}(\text{ClO}_4)_3$  solutions were excited with the  $514.532 \text{ nm}$   $\text{Ar}^+$  line and only the most dilute solution could be reliably measured.

After passing the spectrometer in subtractive mode, with gratings of 1800 grooves/mm, the scattered light was detected with a cooled CCD detector. The scattering geometries  $I_{\text{VV}} = (\text{X}[\text{ZZ}]\text{Y})$  and  $I_{\text{VH}} = (\text{X}[\text{ZX}]\text{Y})$  are defined as follows: the propagation (wave vector direction) of the exciting laser beam is in X direction and the propagation of the observed scattered light is in Y direction, the  $90^\circ$  geometry. The polarisation (electrical field vector) of the laser beam is fixed in Z direction (vertical) and the polarisation of the observed scattered light is observed in Z direction (vertical) for the  $I_{\text{VV}}$  scattering geometry. For  $I_{\text{VH}}$  the electric field vector of the exciting laser beam is in Z direction (vertical) and the observed scattering light is polarized in the X direction (horizontal). Thus, for the two scattering geometries it follows:

$$I_{\text{VV}} = I(\text{X}[\text{ZZ}]\text{Y}) = 45\bar{\alpha}'^2 + 4\gamma'^2, \quad (1)$$

$$I_{\text{VH}} = I(\text{X}[\text{ZX}]\text{Y}) = 3\gamma'^2, \quad (2)$$

The symbols  $\bar{\alpha}'$  and  $\gamma'$  are the isotropic and the anisotropic invariant of the Raman polarizability tensor, respectively [19]. The isotropic spectrum ( $I_{\text{iso}}$ ) was constructed according to Equation (3):

$$I_{\text{iso}} = I_{\text{VV}} - 4/3I_{\text{VH}}, \quad (3)$$

The polarization degree of the Raman bands,  $\rho$  ( $\rho = I_{\text{VH}}/I_{\text{VV}}$ ) was determined using an analyzer and adjusted, if necessary, before each measuring cycle using  $\text{CCl}_4$  [19].

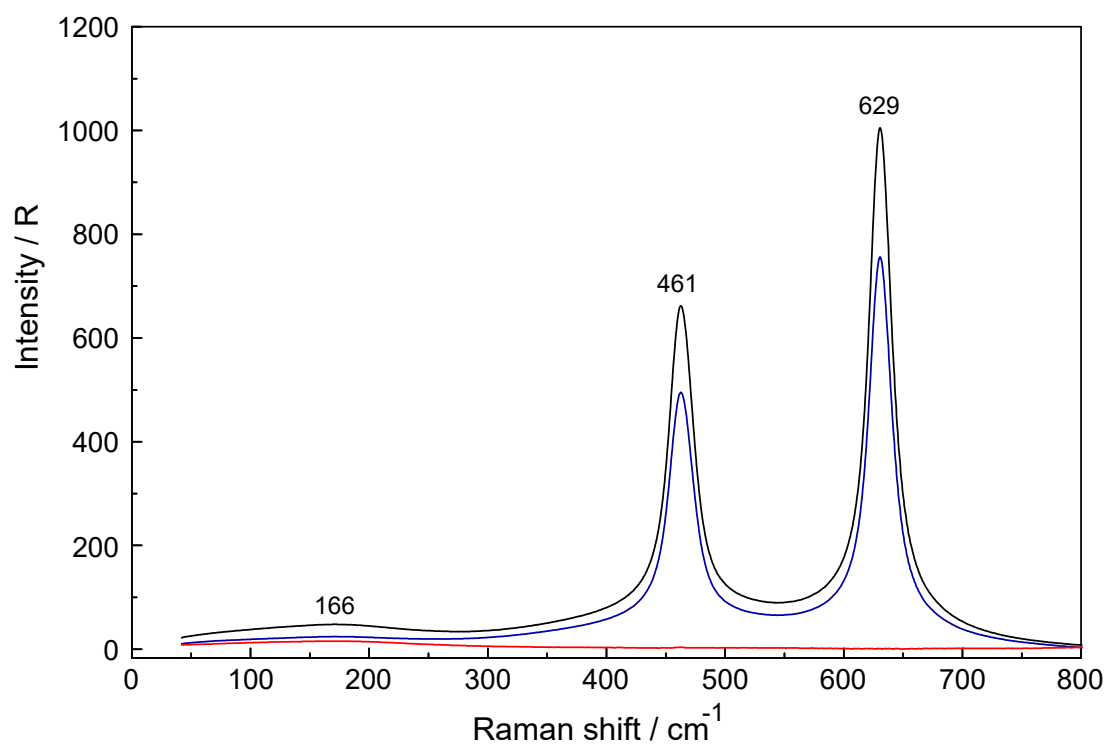
The calibration of the Raman spectra has been carried out using plasma lines [19]. The accuracy of the peak positions for the perchlorate deformation modes were not better than  $\pm 0.5 \text{ cm}^{-1}$  and for the much narrower  $\nu_1(\text{a}_1)\text{ClO}_4^-$  band  $\pm 0.2 \text{ cm}^{-1}$ . The peak positions of the bands were determined by fitting the baseline corrected bands with a Gauss-Lorentz product function (see ref. [20]). The accuracy of the weak and much broader  $\nu_1 \text{ Ln-OH}_2/\text{OD}_2$  bands was  $\pm 1 \text{ cm}^{-1}$  using the perchlorate band at  $461 \text{ cm}^{-1}$  as an internal reference band.

In order to characterize the spectral features in the low wave number region, the Raman spectra in I-format were reduced and the R-spectra obtained. The  $R(\tilde{\nu})$  spectra are independent of the excitation wavenumber  $\tilde{\nu}_L$  and the measured Stokes intensity is further corrected for the scattering factor  $(\nu_L - \tilde{\nu})^3$ . (The scattering factor must be to the power of 3 when applying counting methods [21].) The spectra were further corrected for the Bose-Einstein temperature factor,  $B = [1 - \exp(-h\tilde{\nu}c/kT)]$  and the frequency factor,  $\tilde{\nu}$ , to give the so-called reduced spectrum,  $R(\tilde{\nu})$  (detailed in earlier publications [19,20]). The isotropic spectrum in R-format,  $R_{\text{iso}}$ , is calculated according to equation 3 but substituting the spectra in I-format,  $I_{\text{VV}}$  and  $I_{\text{VH}}$  with  $R_{\text{VV}}$  and  $R_{\text{VH}}$ . In the low wavenumber region, the  $I(\bar{\nu})$  and  $R(\bar{\nu})$  spectra are significantly different and only the spectra in R-format are presented. An advantage in applying isotropic R-spectra is the almost flat baseline in the terahertz region allowing relatively unperturbed observation of any weak modes present.

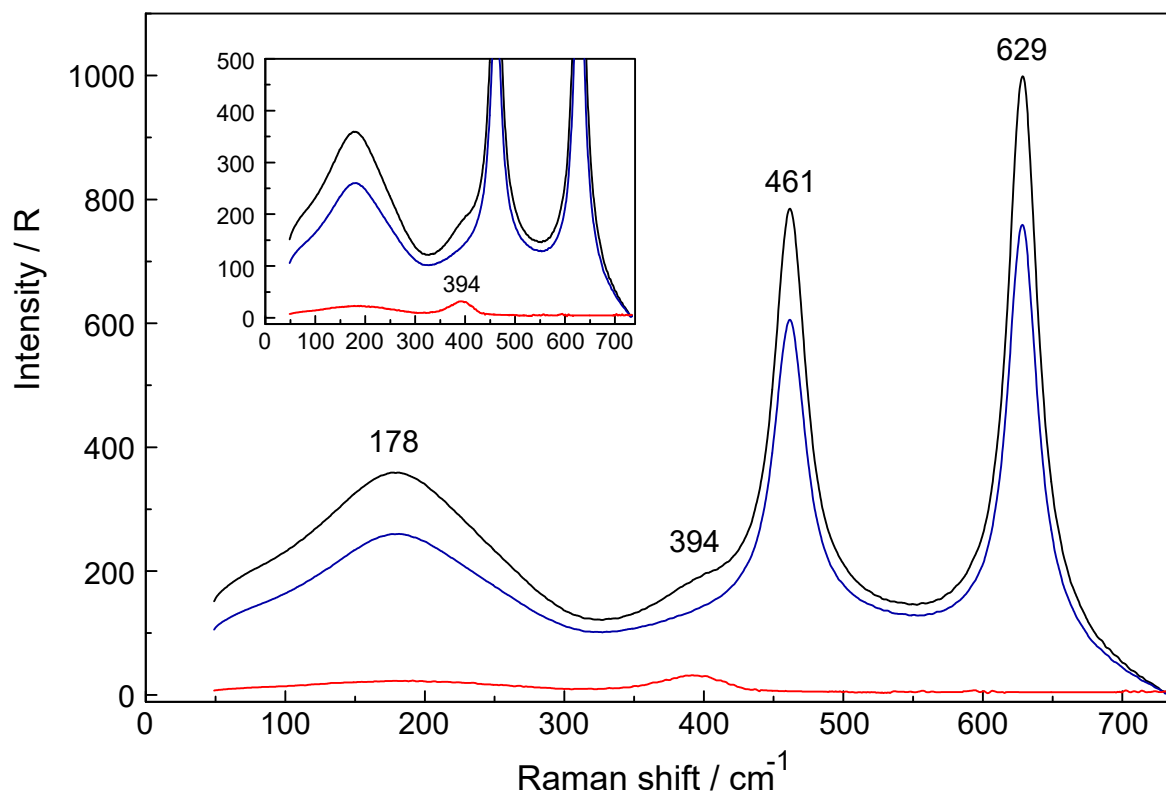
### 3. Results and Discussion

#### 3.1. Raman Spectra on Aqueous $\text{Ln}(\text{ClO}_4)_3$ Solutions ( $\text{Ln} = \text{Lu}^{3+}, \text{Yb}^{3+}, \text{Tm}^{3+}, \text{Er}^{3+}$ and $\text{Ho}^{3+}$ )

The perchlorate spectrum,  $\text{ClO}_4^-(\text{aq})$ : The Raman spectrum of the perchlorate ion in aqueous solution ( $\text{NaClO}_4(\text{aq})$ ) has been well characterized and only a brief description shall be given [14–16]. The  $\text{ClO}_4^-$  ion possesses  $T_d$  symmetry and has nine modes of internal vibrations spanning the representation  $\Gamma_{\text{vib}}(T_d) = \text{a}_1(\text{Ra}) + \text{e}(\text{Ra}) + 2\text{f}_2(\text{Ra}, \text{i.r.})$ . All normal modes are Raman active, but in i.r. only the  $\text{f}_2$  modes are allowed. The  $\nu_1(\text{a}_1) \text{ClO}_4^-$  band, centred at  $931.5 \text{ cm}^{-1}$ , is totally polarized ( $\rho = 0.005$ ) whereas  $\nu_3(\text{f}_2) \text{ClO}_4^-$ , centred at  $1108 \text{ cm}^{-1}$ , is depolarized. The deformation modes  $\nu_4(\text{f}_2) \text{ClO}_4^-$  at  $629 \text{ cm}^{-1}$  and  $\nu_2(\text{e}) \text{ClO}_4^-$  at  $461 \text{ cm}^{-1}$  [15] are also depolarized. In dilute aqueous  $\text{NaClO}_4$  solutions, the spectrum of  $\text{ClO}_4^-(\text{aq})$  shows no sign of contact ion pairs or outer-sphere ion pairs; the  $\nu_1(\text{a}_1) \text{ClO}_4^-$  band at  $931.5 \text{ cm}^{-1}$  is quite narrow with a full width at half height (fwhh) =  $7.2 \text{ cm}^{-1}$ . However, the  $\nu_1(\text{a}_1) \text{ClO}_4^-$  band shows an intrinsic low frequency shoulder at  $923 \text{ cm}^{-1}$  which is caused by Fermi resonance of the overtone of  $\nu_2(\text{e}) \text{ClO}_4^-$ ,  $2 \times \nu_2(\text{e}) = 923 \text{ cm}^{-1}$  with  $\nu_1(\text{a}_1) \text{ClO}_4^-$  band [15]. The antisymmetric stretching mode,  $\nu_3(\text{f}_2) \text{ClO}_4^-$ , is much weaker in intensity than  $\nu_1(\text{a}_1)$  and it appears at  $1106 \text{ cm}^{-1}$  with a fwhh =  $65 \text{ cm}^{-1}$ . In Figure 1A the scattering profiles in R-format ( $R_{\text{VV}}$ ,  $R_{\text{VH}}$ , and  $R_{\text{iso}}$ ) of a  $3.801 \text{ mol}\cdot\text{L}^{-1}$   $\text{NaClO}_4(\text{aq})$  are presented from 50 to  $800 \text{ cm}^{-1}$  and in addition the overview Raman scattering profiles ( $I_{\text{VV}}$ ,  $I_{\text{VH}}$  and  $I_{\text{iso}}$ ) from 50 to  $1800 \text{ cm}^{-1}$  are given in Figure S1 together with the band positions and assignments.



(A)



(B)

Figure 1. Cont.

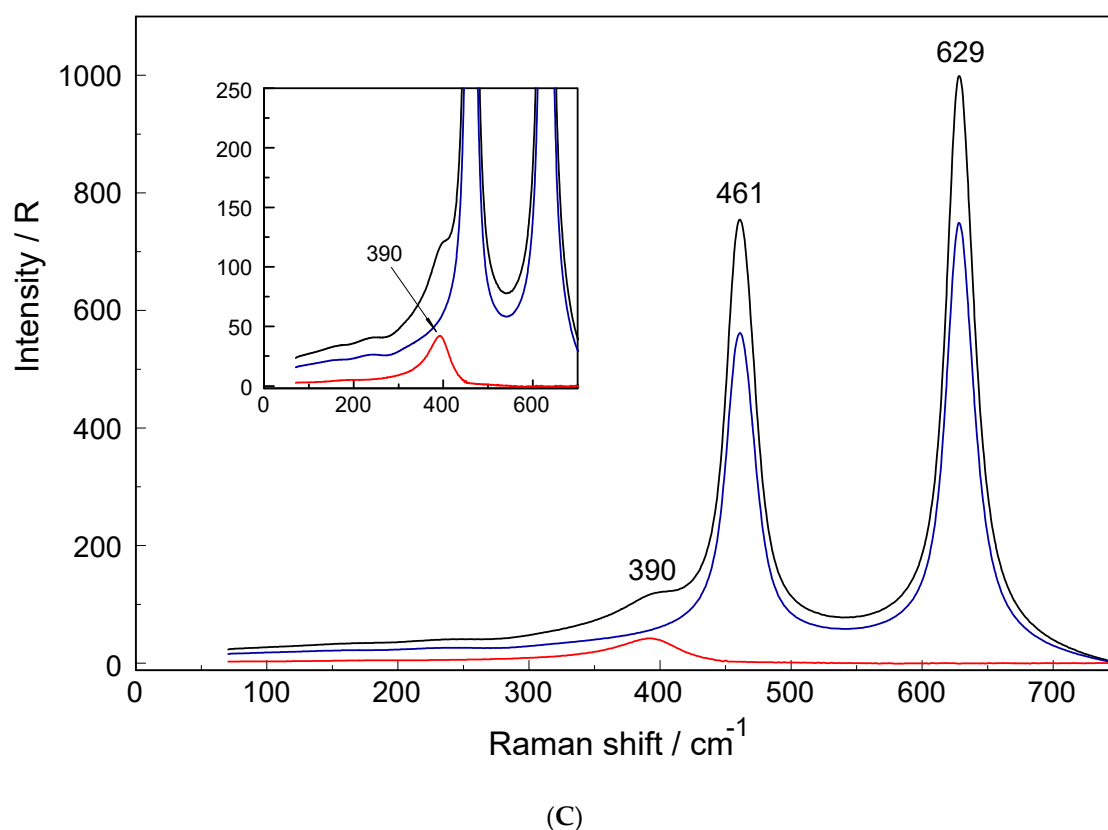


**Figure 1.** (A). Raman scattering profiles in R-format (from top to bottom:  $R_{VV}$  (black),  $R_{VH}$  (blue) and  $R_{iso}$  (red)) of a  $3.801 \text{ mol}\cdot\text{L}^{-1}$   $\text{NaClO}_4(\text{aq})$  solution ( $R_W = 12.05$ ). Note the broad weak mode at  $166 \text{ cm}^{-1}$  is due to the restricted translation of the O-H...H unit of the water molecules. The much larger, depolarized modes at  $461 \text{ cm}^{-1}$  and  $629 \text{ cm}^{-1}$  are the deformation modes of perchlorate,  $\text{ClO}_4^- (\text{aq})$ . (B). A  $\text{Yb}(\text{ClO}_4)_3$  solution spectrum at  $0.240 \text{ mol}\cdot\text{L}^{-1}$  ( $R_W = 226.6$ ) in R-format (spectra from top to bottom:  $R_{VV}$  (black),  $R_{VH}$  (blue) and  $R_{iso}$  (red)). The inset shows the  $R_{iso}$  spectrum in greater detail. Note the broad and weak  $\nu_1 \text{YbO}_8$  stretching mode at  $394 \text{ cm}^{-1}$  (fwhh =  $52 \text{ cm}^{-1}$ ) of the  $[\text{Yb}(\text{OH}_2)_8]^{3+}$  species. The much larger, depolarized bands at  $461 \text{ cm}^{-1}$  and  $629 \text{ cm}^{-1}$  are the deformation modes of perchlorate,  $\text{ClO}_4^- (\text{aq})$ . (C). Raman scattering profiles of a  $\text{Yb}(\text{ClO}_4)_3$  solution at  $2.423 \text{ mol}\cdot\text{L}^{-1}$  in R-format (spectra from top to bottom:  $R_{VV}$  (black),  $R_{VH}$  (blue) and  $R_{iso}$  (red)). The inset shows the  $R_{iso}$  spectrum in greater detail. Note the broad and weak  $\nu_1 \text{YbO}_8$  stretching mode at  $390 \text{ cm}^{-1}$  of the  $[\text{Yb}(\text{OH}_2)_8]^{3+}$  species. The much larger, depolarized bands at  $461 \text{ cm}^{-1}$  and  $629 \text{ cm}^{-1}$  are the deformation modes of perchlorate,  $\text{ClO}_4^- (\text{aq})$ .

The Raman spectra of  $\text{Lu}(\text{ClO}_4)_3(\text{aq})$ ,  $\text{Yb}(\text{ClO}_4)_3(\text{aq})$ ,  $\text{Tm}(\text{ClO}_4)_3(\text{aq})$ ,  $\text{Er}(\text{ClO}_4)_3(\text{aq})$  and  $\text{Ho}(\text{ClO}_4)_3(\text{aq})$ : First, we present and discuss the spectroscopic results on  $\text{Yb}(\text{ClO}_4)_3$  followed below by the spectra of aqueous  $\text{Tm}(\text{ClO}_4)_3$ ,  $\text{Er}(\text{ClO}_4)_3$  and  $\text{Ho}(\text{ClO}_4)_3$  solutions. The Raman spectra of aqueous  $\text{Lu}(\text{ClO}_4)_3$  solutions have been reported recently [17] with the  $\nu_1 \text{LuO}_8$  breathing mode at  $396 \text{ cm}^{-1}$ .

Figure 1B,C show the scattering profiles of aqueous  $\text{Yb}(\text{ClO}_4)_3$  solutions at  $0.240 \text{ mol}\cdot\text{L}^{-1}$  ( $R_W = 226.6$ ) and, in comparison, a solution at  $2.423 \text{ mol}\cdot\text{L}^{-1}$  ( $R_W = 16.86$ ) respectively. The Raman scattering profiles of the  $0.240 \text{ mol}\cdot\text{L}^{-1}$  aqueous  $\text{Yb}(\text{ClO}_4)_3$  solution (Figure 1B) from  $40$ – $750 \text{ cm}^{-1}$  shows two  $\text{ClO}_4^- (\text{aq})$  bands at  $461 \text{ cm}^{-1}$  and  $629 \text{ cm}^{-1}$  and a broad, weak polarized mode (isotropic scattering) at  $394 \text{ cm}^{-1}$  which does not occur in  $\text{NaClO}_4(\text{aq})$ . Therefore, the band at  $394 \text{ cm}^{-1}$  has to be assigned to the  $\nu_1 \text{YbO}_8$  breathing mode of the  $[\text{Yb}(\text{H}_2\text{O})_8]^{3+}$  species. In the at  $2.423 \text{ mol}\cdot\text{L}^{-1}$  ( $R_W = 16.86$ )  $\text{Yb}(\text{ClO}_4)_3$  solution (Figure C), however, the  $\nu_1 \text{YbO}_8$  breathing mode is shifted by  $4 \text{ cm}^{-1}$  to lower wavenumbers compared to the dilute solution (Figure 1B). An overview Raman spectrum of the  $2.423 \text{ mol}\cdot\text{L}^{-1}$   $\text{Yb}(\text{ClO}_4)_3$  solution is given in Figure S2 (top panel) from  $80$ – $1400 \text{ cm}^{-1}$  which displays all

four perchlorate bands and the weak isotropic mode at  $390\text{ cm}^{-1}$  assigned to the  $\nu_1$   $\text{YbO}_8$  breathing mode. The vibrational bands in the anisotropic scattering could only be detected in the concentrated  $\text{Yb}(\text{ClO}_4)_3$  solution at  $2.423\text{ mol}\cdot\text{L}^{-1}$  because of their very weak and broad nature. These anisotropic bands are even weaker than the already weak  $\nu_1$   $\text{YbO}_8$  breathing mode with an integrated band intensity at 3161. The band fit results for the anisotropic scattering are given in Table S1 and presented in Figure 2. Five bands appear at  $88.5\text{ cm}^{-1}$  (fwhh = 119),  $158.7\text{ cm}^{-1}$  (fwhh =  $97.6.9\text{ cm}^{-1}$ ),  $229.4\text{ cm}^{-1}$  (fwhh =  $75.7\text{ cm}^{-1}$ ),  $260.0\text{ cm}^{-1}$  (fwhh =  $68\text{ cm}^{-1}$ ) and  $333.2\text{ cm}^{-1}$  (fwhh = 85.3) in the anisotropic scattering in the  $2.423\text{ mol}\cdot\text{L}^{-1}$   $\text{Yb}(\text{ClO}_4)_3(\text{aq})$  solution. These weak, broad bands stem from the  $\text{YbO}_8$  skeleton fundamentals of the  $[\text{Yb}(\text{OH}_2)_8]^{3+}$  species and break the symmetry of the  $\text{YbO}_8$  skeleton. Therefore, they appear only in the anisotropic scattering, but not in the isotropic profile. From group theoretical considerations we expect 7 Raman active modes for the  $\text{YbO}_8$  skeleton (ligated water molecules seen as point masses) and a brief group theoretical discussion shall be given. The  $\text{YbO}_8$  skeleton ( $D_{4d}$  symmetry) with its 9 atoms leads to 21 normal modes and the irreducible representation follows as:  $\Gamma_v(D_{4d}) = 2a_1(\text{Ra}) + b_1(\text{i.a.}) + 2b_2(\text{i.r.}) + 3e_1(\text{i.r.}) + 3e_2(\text{Ra}) + 2e_3(\text{Ra})$ . (The  $\text{YbO}_8$  skeleton possesses no symmetry centre but the mutual exclusion rule nevertheless applies.) Seven modes with the character  $a_1$ ,  $e_2$  and  $e_3$  are Raman allowed while six modes with the character  $b_1$ ,  $b_2$  and  $e_1$  are i.r. active. The totally symmetric  $\text{Yb-O}$  stretch, the breathing mode, is only Raman active and appears strongly polarized in the Raman spectrum as the strongest band of the  $\text{YbO}_8$  skeleton. Two additional depolarized Raman stretching modes are expected (character  $e_2$  and  $e_3$ ) as well as four other Raman deformation modes (character  $a_1$ ,  $e_2$  and  $e_3$ ). In infrared, two stretching modes (character  $b_2$  and  $e_1$ ) are expected and the remaining are deformations. In reality, however, we observe only six skeleton modes with one unaccounted mode (see also [17]). From our Raman spectroscopic results, it follows directly that the  $\text{Yb}^{3+}\text{-OH}_2$  hydration shell cannot constitute a hexa-hydrate ( $T_h$  symmetry) which has been, for instance, characterized for  $[\text{Al}(\text{OH}_2)_6]^{3+}(\text{aq})$  [22,23]. Group theoretical considerations expect only three skeleton modes in Raman for  $[\text{Al}(\text{OH}_2)_6]^{3+}$ ; one of which should be totally polarized (breathing mode for the  $\text{AlO}_6$  skeleton) and the remaining two depolarized. All of these bands were detected in the Raman spectrum of an  $\text{Al}(\text{ClO}_4)_3(\text{aq})$  solution with the symmetric stretching mode of  $[\text{Al}(\text{OH}_2)_6]^{3+}$  at  $525\text{ cm}^{-1}$  strongly polarized and two bands at  $438\text{ cm}^{-1}$  and  $332\text{ cm}^{-1}$  which are depolarized [22,23].

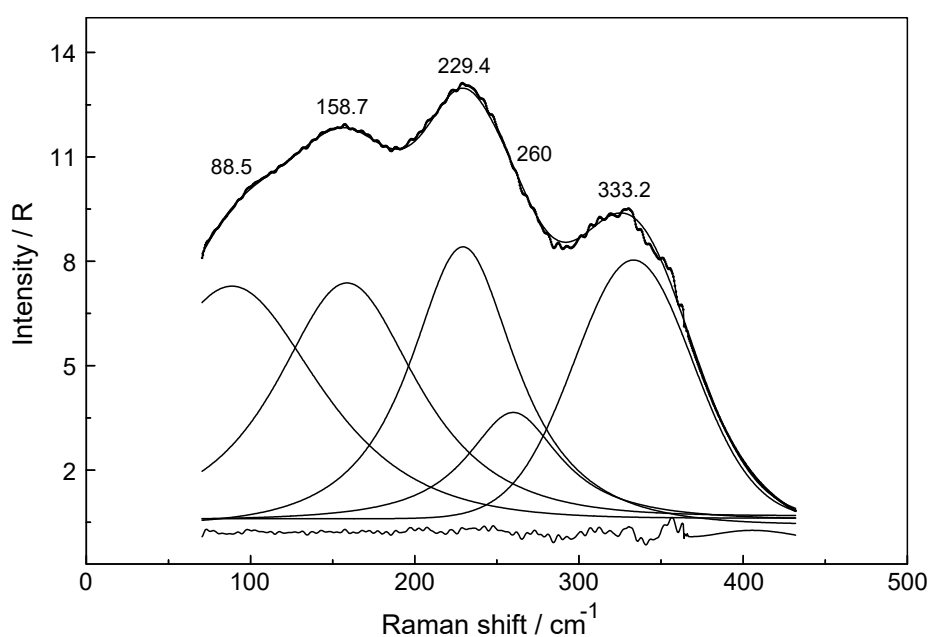


**Figure 2.** Result of a band fit of an anisotropic Raman scattering profile of a  $\text{Yb}(\text{ClO}_4)_3$  solution at  $2.423\text{ mol}\cdot\text{L}^{-1}$  in R-format. Shown are the measured spectrum, baseline corrected, the sum curve of the band fit and the band components. Underneath is the residue curve, which is the difference of the measured spectrum and the sum curve.

The concentration dependence of the band parameters (peak positions, full width at half height (fwhh) and integrated band areas) of the  $\nu_1$  YbO<sub>8</sub> breathing mode for Yb(ClO<sub>4</sub>)<sub>3</sub> solutions allows the determination of the change of these band parameters as a function of concentration. The band profiles of the  $\nu_1$  YbO<sub>8</sub> breathing mode are given in Figure 3 at concentrations 0.240 mol·L<sup>-1</sup> ( $R_W = 268.74$ ), 0.603 mol·L<sup>-1</sup> ( $R_W = 85.17$ ), 0.808 mol·L<sup>-1</sup> ( $R_W = 62.13$ ), 1.217 mol·L<sup>-1</sup> ( $R_W = 16.86$ ) and finally at 2.423 mol·L<sup>-1</sup> ( $R_W = 16.86$ ). The  $\nu_1$ Yb–O breathing mode appears at 394 cm<sup>-1</sup> at the lowest concentrations and shifts  $\sim 4$  cm<sup>-1</sup> to lower wavenumbers at the highest concentration. Furthermore, the bandwidths also increase with increasing solute concentration from 52 cm<sup>-1</sup> for the 0.240 mol·L<sup>-1</sup> solution to 59 cm<sup>-1</sup> for the 2.423 mol·L<sup>-1</sup> solution (Figure 3). This slight change in band parameters of  $\nu_1$  YbO<sub>8</sub> breathing mode with increasing solute concentration may be due to ion pair formation in concentrated solutions (The ion pairing effect in perchlorate solutions is discussed in detail in [15,17]). The integrated band intensity of the  $\nu_1$ YbO<sub>8</sub> breathing mode,  $A_{394}$ , rises linearly with the solution concentration. The dependence of the integrated band intensity of the  $\nu_1$  YbO<sub>8</sub> breathing mode of [Yb(OH<sub>2</sub>)<sub>8</sub>]<sup>3+</sup> as a function of the Yb(ClO<sub>4</sub>)<sub>3</sub> concentration is given in Figure S3 and for the linear relationship follows:  $A_{394} = 1303.7 \cdot C_{\text{Yb}(\text{ClO}_4)_3}$  ( $R^2 = 99.9$ ).

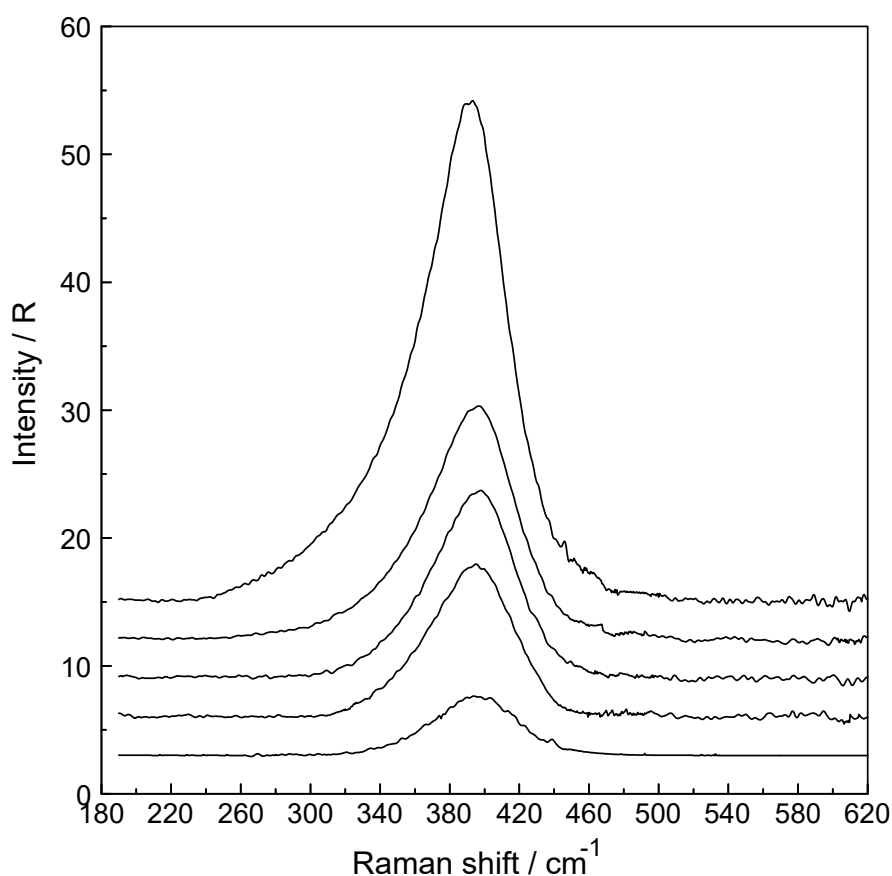


**Figure 3.** Stack plot of five isotropic Raman profiles in R-format of aqueous Yb(ClO<sub>4</sub>)<sub>3</sub> solution. From bottom to top: at 0.240 mol·L<sup>-1</sup>, 0.603 mol·L<sup>-1</sup>, 0.808 mol·L<sup>-1</sup>, 1.217 mol·L<sup>-1</sup> and 2.423 mol·L<sup>-1</sup>.

In addition to the  $\nu_1$ YbO<sub>8</sub> of [Yb(OH<sub>2</sub>)<sub>8</sub>]<sup>3+</sup> an extremely weak and broad band centered at  $170 \pm 10$  cm<sup>-1</sup> appears isotropic Raman scattering in of aqueous Yb(ClO<sub>4</sub>)<sub>3</sub> solution (see Figure S2, top panel). This isotropic band is assigned to a restricted translational mode of the weakly H-bonded water molecules (O–H⋯OClO<sub>3</sub><sup>-</sup>). The mode is strongly anion and concentration-dependent [14–16]. The influence of the ClO<sub>4</sub><sup>-</sup> on the water spectrum has been discussed in recent studies on aqueous Ln(ClO<sub>4</sub>)<sub>3</sub> solutions [14–17]. The Raman scattering profiles,  $I_{VV}$ ,  $I_{VH}$  and  $I_{iso}$  of the O–H stretching



region of H<sub>2</sub>O and its bending mode of a Yb(ClO<sub>4</sub>)<sub>3</sub> solution at 2.423 mol·L<sup>-1</sup> and their peak positions are given in Figure S2, bottom panel, and for details see [14–16].

The triflate ion (trifluoromethanesulfonate) in aqueous solution acts as an even weaker complex forming anion and is suited, therefore, for studying metal ion hydration. In aqueous solution, however, the weak  $\nu_1$  band of [Yb(OH<sub>2</sub>)<sub>8</sub>]<sup>3+</sup> at ~394 cm<sup>-1</sup> is overlapped by a strongly polarized triflate band at 319 cm<sup>-1</sup> and so band fit analysis was applied. The isotropic Raman spectrum of Yb(CF<sub>3</sub>SO<sub>3</sub>)<sub>3</sub>(aq) at 1.25 mol·L<sup>-1</sup> is shown in Figure S4 and the band fit analysis gave two bands with the first band component at 319 cm<sup>-1</sup> and the second band at 394 cm<sup>-1</sup> (fwhh = 50 cm<sup>-1</sup>). The first band, a polarized band, stems from CF<sub>3</sub>SO<sub>3</sub><sup>-</sup> (aq) but the second band is the  $\nu_1$  YbO<sub>8</sub> breathing mode of [Yb(H<sub>2</sub>O)<sub>8</sub>]<sup>3+</sup>. Band parameters and assignments of CF<sub>3</sub>SO<sub>3</sub><sup>-</sup> (aq) modes are given in [16].

The effect of deuteration on the YbO<sub>8</sub> skeleton modes of [Yb(OD<sub>2</sub>)<sub>8</sub>]<sup>3+</sup> was studied in Yb(ClO<sub>4</sub>)<sub>3</sub><sup>-</sup>D<sub>2</sub>O solution and resulted in a shift of the Yb–OD<sub>2</sub> mode down to 374 cm<sup>-1</sup>. The shift of  $\nu_1$  on deuteration is given as  $\nu_1' = \nu_1 [m(\text{H}_2\text{O})/m(\text{D}_2\text{O})]^{1/2} = (394\text{cm}^{-1}) \cdot \sqrt{18.02/20.03} = 0.9485 \times 394\text{ cm}^{-1} = 373.7\text{ cm}^{-1}$ . (The water and heavy water molecules are taken as point masses.) A Raman spectra of Yb(ClO<sub>4</sub>)<sub>3</sub> solutions in D<sub>2</sub>O at 0.779 mol·L<sup>-1</sup> is presented in Figure 4 and for a concentration at 1.276 mol·L<sup>-1</sup> in Figure S5. This isotope shift of the symmetrical stretch of YbO<sub>8</sub> in changing from [Yb(OH<sub>2</sub>)<sub>8</sub>]<sup>3+</sup> (H<sub>2</sub>O) to [Yb(OD<sub>2</sub>)<sub>8</sub>]<sup>3+</sup> (D<sub>2</sub>O) and the totally symmetric character of the mode, that is, showing a polarization degree ~0, are indeed proof for the character of this mode.

In the Raman spectra of the Tm(ClO<sub>4</sub>)<sub>3</sub>, Er(ClO<sub>4</sub>)<sub>3</sub> and Ho(ClO<sub>4</sub>)<sub>3</sub> solutions appear also as strongly polarized bands and were observed at 391, 389 cm<sup>-1</sup>, and 387 cm<sup>-1</sup> respectively. These isotropic bands are unique in these HRE ion solutions and cannot be found in the hydrated ClO<sub>4</sub><sup>-</sup> (aq) spectrum.

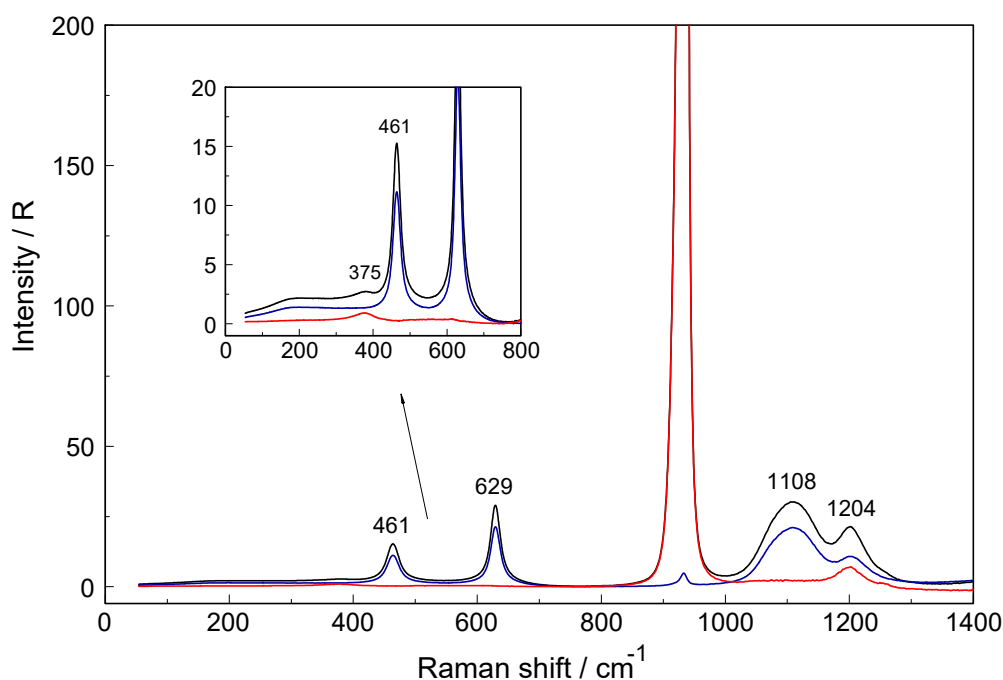


**Figure 4.** Raman scattering profiles in R-format (spectra from top to bottom:  $R_{VV}$ ,  $R_{VH}$  and  $R_{iso}$ ) of a 0.779 mol·L<sup>-1</sup> Yb(ClO<sub>4</sub>)<sub>3</sub> solution in D<sub>2</sub>O. The inset shows the low frequency region in larger detail. The weak band at 375 cm<sup>-1</sup> is assigned to the Yb–OD<sub>2</sub> mode of the YbO<sub>8</sub> skeleton which is shifted due to the isotope effect by changing from H<sub>2</sub>O to D<sub>2</sub>O (see also Figure 1B). Note the band at 1204 cm<sup>-1</sup> which is due to the deformation mode of D<sub>2</sub>O.

The representative Raman spectra of Tm(ClO<sub>4</sub>)<sub>3</sub>, Er(ClO<sub>4</sub>)<sub>3</sub> and Ho(ClO<sub>4</sub>)<sub>3</sub> solutions are given in Figures S6–S8, respectively. Several concentrations of the Tm(ClO<sub>4</sub>)<sub>3</sub>(aq) were measured but from the coloured Er(ClO<sub>4</sub>)<sub>3</sub> and Ho(ClO<sub>4</sub>)<sub>3</sub> solutions only the dilute solutions could be reliably measured.

(Concentrated  $\text{Er}(\text{ClO}_4)_3$  and  $\text{Ho}(\text{ClO}_4)_3$  solutions absorb the laser light markedly.) The peak positions for the  $\nu_1$   $\text{LnO}_8$  breathing modes for  $[\text{Lu}(\text{OH}_2)_8]^{3+}$  (taken from [17]),  $[\text{Yb}(\text{OH}_2)_8]^{3+}$ ,  $[\text{Tm}(\text{OH}_2)_8]^{3+}$ ,  $[\text{Er}(\text{OH}_2)_8]^{3+}$  and  $[\text{Ho}(\text{OH}_2)_8]^{3+}$  are given in Table 1. Force constant calculations for the  $\nu_1$   $\text{LnO}_8$  breathing modes of this species, applying a simple model, have been carried out according to equation (4):

$$k_{\text{M-O}} = 4\pi^2 c^2 \tilde{\nu}_i^2 N^{-1} A_L, \quad (4)$$

with  $c$ , the velocity of light,  $\tilde{\nu}_i$  the wavenumber of the mode  $i$ ,  $N$  the Avogadro constant and  $A_L$  the molecular weight of the ligand, in our case water. The force constants,  $k_{\text{Ln-O}}$ , calculated for the measured  $\nu_1$  breathing modes are given in Table 1 together with the corresponding  $\text{Ln}^{3+}$ -O bond distances [7]. The force constants increase from  $\text{Lu}^{3+}$ ,  $\text{Yb}^{3+}$ ,  $\text{Tm}^{3+}$ ,  $\text{Er}^{3+}$  and  $\text{Ho}^{3+}$  in the same order as the corresponding  $\text{Ln-O}$  bond distances decrease, namely  $\text{Lu-O} < \text{Yb-O} < \text{Tm-O} < \text{Er-O} < \text{Ho-O}$  (Figure S9).

**Table 1.** Band parameters such as peak positions,  $\nu_1$ , force constants,  $k_{\text{Ln-O}}$ , the full width at half heights, and the scattering intensities for the  $\text{Ln-O}$  breathing mode of  $\text{Ho}^{3+}$ ,  $\text{Er}^{3+}$ ,  $\text{Tm}^{3+}$ ,  $\text{Yb}^{3+}$  and  $\text{Lu}^{3+}$  for the  $[\text{Ln}(\text{OH}_2)_8]^{3+}$  species at 22 °C. Furthermore, the literature data for the water exchange [24] and the  $\text{Ln-O}$  bond distances [7] for these  $[\text{Ln}(\text{OH}_2)_8]^{3+}$  species are given.

$[\text{Ln}(\text{OH}_2)_8]^{3+}$	$\nu_1$ $\text{Ln-O}$ / $\text{cm}^{-1}$	$k_{\text{Ln-O}}/\text{Nm}^{-1}$	Fwhh/ $\text{cm}^{-1}$	$S_h$	$k_{\text{ex}}^{298}/10^8 \text{ s}^{-1}$ a)	$\tau_w/\text{ns}$	$\text{Ln-O}/\text{\AA}$ b)
$\text{Ho}^{3+}$	387	158.97	55	0.0170	1.91	5.24	2.379
$\text{Er}^{3+}$	389	160.62	54	0.0168	1.18	8.48	2.364
$\text{Tm}^{3+}$	391	162.27	53	0.0165	0.81	12.34	2.350
$\text{Yb}^{3+}$	394	164.77	52	0.0160	0.41	24.39	2.324
$\text{Lu}^{3+}$	396	166.45	52	0.0156	-	-	2.316

a) Ref. [24]; - data at 25 °C. b) Ref. [7]; EXAFS data from  $L_3$  edge (one shell fit) on aqueous trifluoromethanesulfonate solutions.

Relative scattering intensities,  $S_h$ , for the  $\nu_1$   $\text{Ln-O}$  breathing modes are also given in Table 1 and for the definitions of the  $S_h$  see ref. [20]. The small scattering intensity values at 0.0156 to 0.0165 for the  $\nu_1$   $\text{Ln-O}$  modes of the HRE octahydrates reflect the fact that the  $\text{Ln-OH}_2$  bonds possess low polarizability and are hard cations [25]. The accuracy of the scattering coefficient is not better than  $\pm 0.0004$  due to the low scattering intensity, the broadness of the modes and the uncertainties in subtracting the baseline. (Note that the  $S_h$  value for the totally symmetric stretching mode,  $\nu_1 \text{Lu-O}$  is  $0.0156 \pm 0.0004$  and the value reported in [17] is too small.)

From ab initio quantum mechanical charge field molecular dynamics studies, the mean  $\text{Ln-O}$  bond distances ( $\text{Ln} = \text{Ho}^{3+}$ ,  $\text{Er}^{3+}$ ,  $\text{Tm}^{3+}$ ,  $\text{Yb}^{3+}$  and  $\text{Lu}^{3+}$ ) of the octahydrates,  $[\text{Ln}(\text{OH}_2)_8]^{3+}$ , average coordination numbers, vibrational frequencies and the corresponding force constants were presented [13]. The authors claimed an “excellent agreement with experimental results” [13] of the computed frequencies with the measured ones in the glassy state [26]. The theoretical force constants for the  $\nu_1$  breathing modes in [13] deviate considerably from our data in Table 1 and do not follow the expected trend given in Figure S9 in going from holmium to lutetium. This trend reflects the steady increase of the force constants of the  $\text{Ln-O}$  breathing modes with decreasing  $\text{Ln-O}$  bond distances in going from holmium to lutetium (Table 1; Figure S9). The force constant for  $\nu_1$   $\text{Er-OH}_2$  breathing mode in [13] was given  $360 \text{ cm}^{-1}$  equal to the one for the  $\nu_1$   $\text{La-OH}_2$  breathing mode of  $[\text{La}(\text{OH}_2)_9]^{3+}$ . However, our recently published datum for the  $\nu_1$   $\text{La-OH}_2$  breathing mode [14,15] is with  $343 \text{ cm}^{-1}$  much smaller. The calculations in [13] are based on the simplified model of a heteronuclear diatomic species but such an assumption may not be correct. The character of the symmetrical normal mode  $\nu_1$  of the  $\text{LnO}_8$  skeleton of the corresponding  $[\text{Ln}(\text{OH}_2)_8]^{3+}$  species reveals that the central cations remain stationary and only the water molecules are involved in the breathing motion without disturbing the symmetry and therefore these normal modes are totally polarized.

It is known from kinetic studies [24,27,28] that the water exchange reactions of the  $[\text{Ln}(\text{OH}_2)_8]^{3+}$  species for the octahydrates are very fast and these ions are known to be labile. From the rate constants,  $k_{\text{ex}}$  at 25 °C, given in Table 1, follow the water residence times, the time the water molecules reside at these cations. The water residence times are in the range of several nanoseconds (see Table 1) which shows that these ions are indeed quite labile. From the vibration periods of the  $\nu_1$  Lu–O modes which are at 0.086 to 0.084 ps in going from holmium(III) to lutetium(III) it follows that these species vibrate several hundred thousand times [17] before one water exchange occurs. Although the HRE ions are labile structures, Raman spectroscopy probes the actual structure of these octahydrate species. (It is worth mentioning that the intramolecular bond exchange rate is only a few picoseconds, much faster than the water exchange reaction, therefore for such labile structures for instance  $[\text{Cu}(\text{OH}_2)_5]^{2+}$  [27], Raman observes an average structure and, so, a single broad mode appears as a result and at higher peak positions than for comparable divalent metal ions.)

### 3.2. $\text{YbCl}_3$ Solutions

From thermodynamic measurements, it is known that  $\text{Lu}^{3+}$  and  $\text{Yb}^{3+}$  form weak chloro-complexes/ion-pairs [29–32]. As a model system for the HRE ion hydrates, aqueous  $\text{YbCl}_3$  solutions were investigated. The polarized, depolarized and isotropic Raman scattering profiles of a 3.224 mol·L<sup>−1</sup>  $\text{YbCl}_3$  solution compared to a solution at 0.802 mol·L<sup>−1</sup> are presented in Figure 5. Furthermore, the isotropic scattering profiles of three  $\text{YbCl}_3(\text{aq})$  solutions at 3.224 mol·L<sup>−1</sup> ( $R_w = 15.64$ ), 1.600 mol·L<sup>−1</sup> ( $R_w = 33.06$ ) and 0.802 mol·L<sup>−1</sup> ( $R_w = 67.55$ ) from 55–700 cm<sup>−1</sup> are given in Figure 6. Two  $\text{YbCl}_3$  solutions in heavy water were also investigated at 0.422 mol·L<sup>−1</sup> and at 0.844 mol·L<sup>−1</sup> and the overview Raman scattering spectra of a 0.422 mol·L<sup>−1</sup>  $\text{YbCl}_3$  solution in  $\text{D}_2\text{O}$  is given in Figure S10. In dilute  $\text{YbCl}_3(\text{aq})$ , the  $\text{Yb}^{3+}$  ion is fully hydrated indicated by the  $\nu_1$  Yb–OH<sub>2</sub> mode at 394 cm<sup>−1</sup> for the  $[\text{Yb}(\text{OH}_2)_8]^{3+}$  species while in dilute  $\text{YbCl}_3$  solution in heavy water at 0.422 mol·L<sup>−1</sup> (see Figure S10), the  $\nu_1$  Yb–OD<sub>2</sub> mode of  $[\text{Yb}(\text{OD}_2)_8]^{3+}$  appears at 376 cm<sup>−1</sup> due to the vibrational isotope effect (see discussion further above; H<sub>2</sub>O/D<sub>2</sub>O are considered point masses).

The  $\nu_1$  Yb–OH<sub>2</sub> stretching mode in the 3.224 mol·L<sup>−1</sup>  $\text{YbCl}_3(\text{aq})$  solution, with a mole ratio of solute to water at 1 to 15.64 appears at 389 cm<sup>−1</sup> and shifts with dilution to higher frequencies (see Figure 5). In a 0.400 mol·L<sup>−1</sup> ( $R_w = 136.98$ )  $\text{YbCl}_3(\text{aq})$  solution the  $\nu_1$  Yb–OH<sub>2</sub> breathing mode appears at 394 cm<sup>−1</sup> with a fwhh at 52 cm<sup>−1</sup> and these band parameters are comparable to the ones in a dilute  $\text{Yb}(\text{ClO}_4)_3(\text{aq})$  solution in which the fully hydrated  $[\text{Yb}(\text{OH}_2)_8]^{3+}$  exists.

A broad isotropic component at 206 cm<sup>−1</sup> and a broad feature at 256 cm<sup>−1</sup> are also observed. The band at 256 cm<sup>−1</sup> is due to the partially hydrated water molecules of the  $[\text{Yb}(\text{OH}_2)_7\text{Cl}]^{2+}$  species. A Yb–Cl stretching mode should appear at much higher frequencies, namely at ~500 cm<sup>−1</sup>, but may be very broad and weak and could not be observed (see spectroscopic and DFT results on  $\text{ZnCl}_2(\text{aq})$  [33]). The isotropic component at 206 cm<sup>−1</sup> is assigned to the restricted translation band of water of its O–H...O/Cl<sup>−</sup> units. These findings are evidence that Cl<sup>−</sup> substitutes water from the first hydration shell of  $\text{Yb}^{3+}$  and a partially hydrated  $\text{Yb}^{3+}$ -chloro-complex formulated as  $[\text{Yb}(\text{OH}_2)_7\text{Cl}]^{2+}$  is formed.

The integrated band intensities of  $\nu_1$  YbO<sub>8</sub> band of the fully hydrated species,  $[\text{Yb}(\text{OH}_2)_8]^{3+}$ , as a function of concentration was determined from quantitative Raman analysis and it turned out that the integrated band intensity,  $A_{394}$ , does not increase linearly with the total  $\text{YbCl}_3$  concentration ( $C_T$ ). However, a linear increase in band intensity would be expected if the  $\text{Yb}^{3+}$  - octahydrate is the only stable species in  $\text{YbCl}_3$  solution and such a linear relationship was observed in  $\text{Yb}(\text{ClO}_4)_3(\text{aq})$  solutions (see Figure S3). The measured integrated band intensity of the  $\nu_1$  YbO<sub>8</sub> band in  $\text{YbCl}_3$  (aq),  $A_{394}$ , follows a linear relationship between  $A_{394}$  and  $C_T$  up to ~0.4 mol·L<sup>−1</sup> but then levels off noticeably at higher  $\text{YbCl}_3$  concentrations (Figure S11). Obviously, above ~0.4 mol·L<sup>−1</sup>  $\text{YbCl}_3$  fractions of the fully hydrated  $\text{Yb}^{3+}$  (aq) are converted to a 1:1  $\text{Yb}^{3+}$  chloro-complex species. The existence of higher chloro complexes than 1:1 can be convincingly ruled out taking into account the results of earlier anion exchange studies on aqueous rare earth chloride systems [32]. The mole fractions of both species are plotted in Figure 7. The fraction of the chloro-complex at 29%, in the most concentrated solution,

is rather small and the fully hydrated species at 71% is still dominant. With dilution, the fraction of the chloro-complex species diminishes quickly and at  $\sim 0.4 \text{ mol}\cdot\text{L}^{-1}$  it is zero.

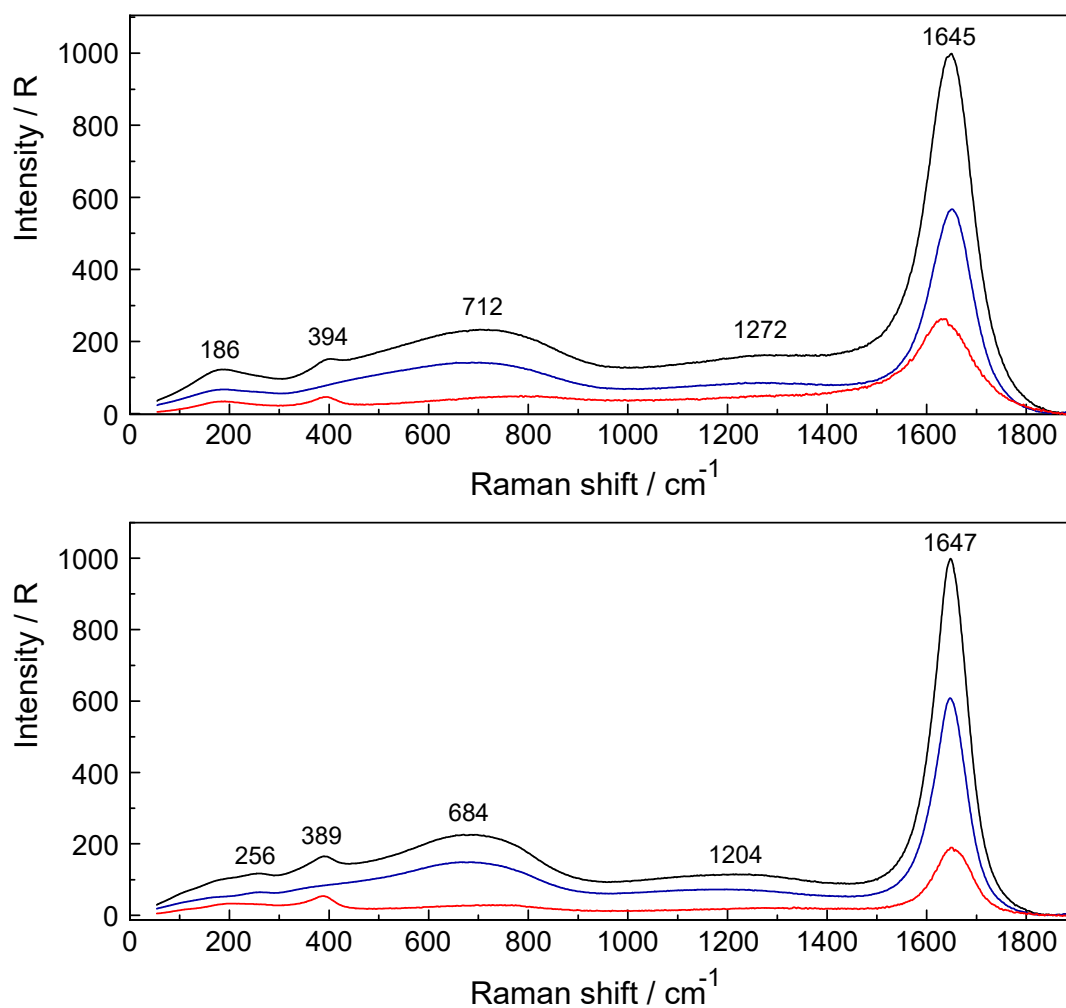


**Figure 5.** Raman scattering profiles ( $R_{VV}$  (black),  $R_{VH}$  (blue) and  $R_{iso}$  (red)) of two  $\text{YbCl}_3(\text{aq})$  solutions from  $55\text{--}1910 \text{ cm}^{-1}$ . Top panel:  $0.802 \text{ mol}\cdot\text{L}^{-1}$ ; Bottom panel:  $3.224 \text{ mol}\cdot\text{L}^{-1}$ .

Shown (Figure 5) is the  $\nu_1 \text{YbO}_8$  symmetric stretching mode at  $394 \text{ cm}^{-1}$  in a  $0.802 \text{ mol}\cdot\text{L}^{-1}$  solution compared to the one at  $389 \text{ cm}^{-1}$  in a  $3.224 \text{ mol}\cdot\text{L}^{-1}$  solution. An additional isotropic band appears at  $256 \text{ cm}^{-1}$  in the  $3.224 \text{ mol}\cdot\text{L}^{-1}$  solution which is due to the stretching mode of the chloro-complex species,  $[\text{Yb}(\text{OH}_2)_7\text{Cl}]^{2+}$  (details in  $R_{iso}$  scattering in the terahertz region see Figure 6). The remaining bands in both panels are due to the water being strongly influenced by the solute at the most concentrated solution. First, in the terahertz region ( $R_{VV}$  scattering), weak, broad bands appear at  $186 \text{ cm}^{-1}$  in the  $0.802 \text{ mol}\cdot\text{L}^{-1}$  solution and at  $202 \text{ cm}^{-1}$  in the  $3.224 \text{ mol}\cdot\text{L}^{-1}$  solution assigned to the restricted translational band of water of the  $\text{O-H}\cdots\text{O}/\text{Cl}^-$  units. Second, very broad bands ( $R_{VV}$  scattering) with peak maxima which appear at  $712 \text{ cm}^{-1}$  ( $0.802 \text{ mol}\cdot\text{L}^{-1}$ ) and  $684 \text{ cm}^{-1}$  ( $3.224 \text{ mol}\cdot\text{L}^{-1}$ ) are due to the librational bands of water. Third, the band at  $1272$  ( $0.802 \text{ mol}\cdot\text{L}^{-1}$ ) and  $1204 \text{ cm}^{-1}$  ( $3.224 \text{ mol}\cdot\text{L}^{-1}$ ) are due to overtones of water librations. Finally, the bands at  $1645$  and  $1647 \text{ cm}^{-1}$  respectively are due to the deformation mode of water,  $\nu_2 \text{H}_2\text{O}$ .

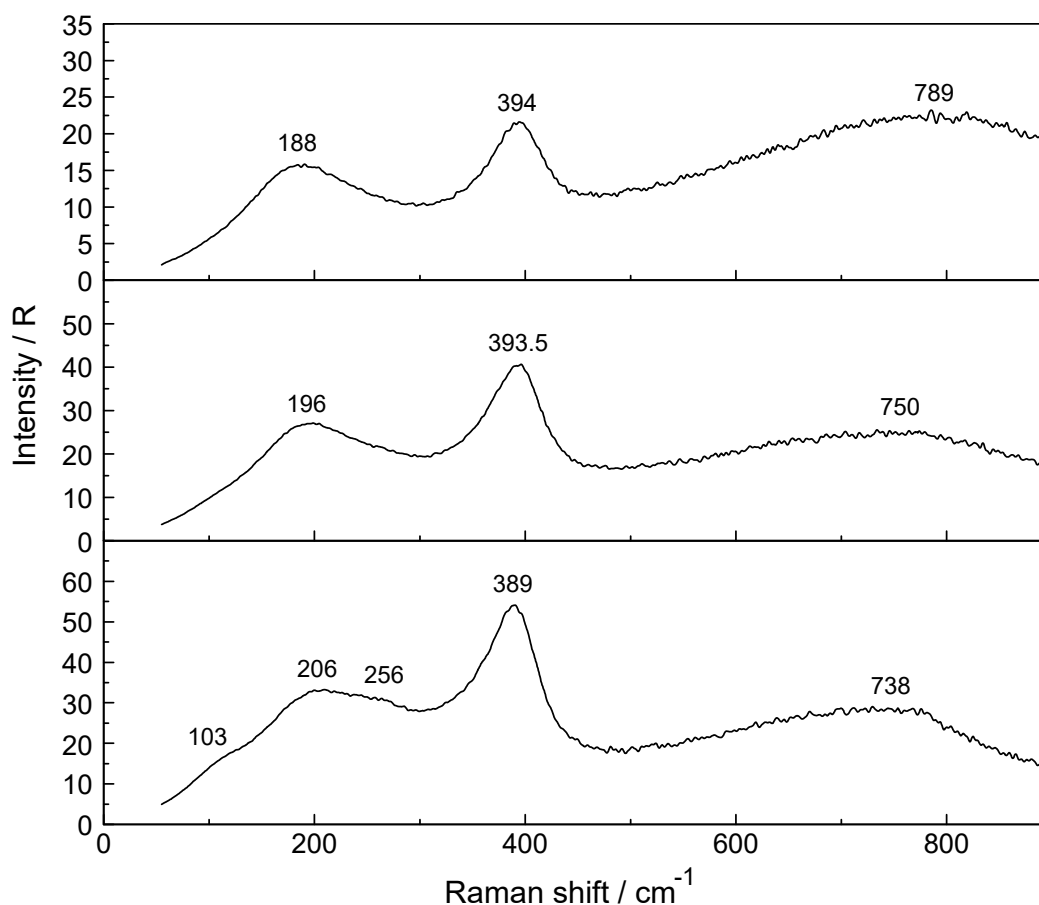
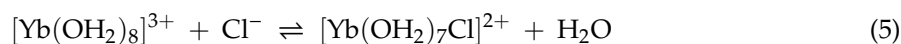


**Figure 6.** Isotropic Raman scattering profiles of  $\text{YbCl}_3(\text{aq})$  solutions from 55–900  $\text{cm}^{-1}$ . From bottom to top: 3.224  $\text{mol}\cdot\text{L}^{-1}$ , 1.600  $\text{mol}\cdot\text{L}^{-1}$  and 0.802  $\text{mol}\cdot\text{L}^{-1}$ . The symmetric  $\text{YbO}_8$  stretching mode appears at 389  $\text{cm}^{-1}$  in a solution at 3.224  $\text{mol}\cdot\text{L}^{-1}$  and is shifted to 393.5  $\text{cm}^{-1}$  in a 0.802  $\text{mol}\cdot\text{L}^{-1}$  solution. The band at 256  $\text{cm}^{-1}$  is due to the stretching mode of the chloro-complex species,  $[\text{Yb}(\text{OH}_2)_7\text{Cl}]^{2+}$ . The restricted translation band of the O-H $\cdots$ O/ $\text{Cl}^-$  band of water shifts from 206  $\text{cm}^{-1}$  in the 3.224  $\text{mol}\cdot\text{L}^{-1}$  solution and appears at 188  $\text{cm}^{-1}$  in the 0.802  $\text{mol}\cdot\text{L}^{-1}$  solution. The broad librational band of water shifts from 738  $\text{cm}^{-1}$  to 789  $\text{cm}^{-1}$  in going from a 3.224  $\text{mol}\cdot\text{L}^{-1}$  solution to the one at 0.802  $\text{mol}\cdot\text{L}^{-1}$ .

The formation of a 1:1 complex with  $\text{Cl}^-$  at higher  $\text{YbCl}_3$  concentrations may be written as:



The formation constant for the 1:1  $\text{Yb}^{3+}$ -chloro-complex,  $K_1$ , may be formulated according to Equation (6):

$$K_1 = \frac{[\text{YbCl}^{2+}]}{[\text{Yb}^{3+}][\text{Cl}^-]} \cdot \frac{f_{\text{YbCl}_2^{2+}}}{f_{\text{Yb}^{3+}} \cdot f_{\text{Cl}^-}} \quad (6)$$

with  $K_1'$  the “concentration quotient” we get:  $K_1 = K_1' \cdot \frac{f_{\text{YbCl}_2^{2+}}}{f_{\text{Yb}^{3+}} \cdot f_{\text{Cl}^-}}$

The concentration quotient can be measured by Raman spectroscopy according to equation (7):

$$K_1' = \frac{(C_T - [\text{Yb}^{3+}])}{[\text{Yb}^{3+}] \cdot [\text{Cl}^-]} \quad (7)$$

where  $C_T$  is the total  $\text{YbCl}_3$  concentration and the concentrations in brackets denote the equilibrium concentrations of the fully hydrated  $\text{Yb}^{3+}$  and  $\text{Cl}^-$ . The equilibrium concentration of  $\text{Yb}^{3+}$  determined by Raman spectroscopy allows us to calculate  $K_1'$ .

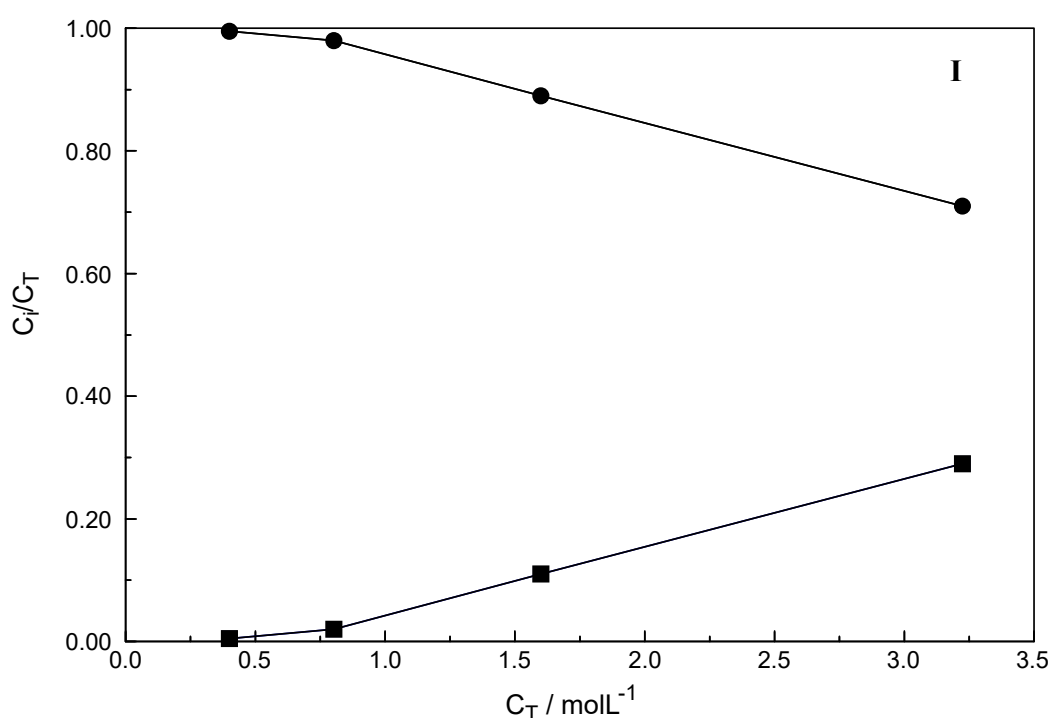


**Figure 7.** Fraction of species detected by quantitative Raman spectroscopy. The filled circles denote the  $[\text{Yb}(\text{OH}_2)_8]^{3+}$ , the fully hydrated  $\text{Yb}^{3+}$  and the filled squares the mono chloro-complex species,  $[\text{Yb}(\text{OH}_2)_7\text{Cl}]^{2+}$ . Note the error bar in the right corner of the graph.

The estimated  $K_1$  value for chloro complex formation in  $\text{YbCl}_3(\text{aq})$  from  $K_1'$  (see ref [17] for details) equal to ca.  $0.06 \pm 0.015$  and a  $\log K_1$  value at ca.  $-1.22$  follows at  $22^\circ\text{C}$ . (Quantitative Raman spectroscopy applied to these solution spectra with weak and broad low frequency bands is not very precise and therefore a higher uncertainty results.) Data from thermodynamic and spectroscopic studies on  $\text{YbCl}_3(\text{aq})$  solutions confirm the weak nature of the complex species [29–32]. The results on aqueous  $\text{LuCl}_3$  solutions and similar rare earth systems [17,29–32] confirm our findings on  $\text{YbCl}_3$  solutions. The chloride ion substitutes a water molecule from the flexible first hydration shell of  $\text{Lu}^{3+}$  and  $\text{Yb}^{3+}$ . With dilution, the weak chloro-complex species dissociates and fully hydrated  $\text{Yb}^{3+}(\text{aq})$  ions detected. This is in contrast to  $\text{AlCl}_3(\text{aq})$  solutions, even in concentrated  $\text{AlCl}_3(\text{aq})$ ,  $\text{Cl}^-$  does not substitute water in the first hydration shell of  $\text{Al}^{3+}$  and it is known that the hydration shell of  $[\text{Al}(\text{OH}_2)_6]^{3+}$  is quite inert [22,23].

The results of an extensive EXAFS study by Allen and co-workers [34] on  $0.1$  and  $0.01 \text{ mol}\cdot\text{L}^{-1}$   $\text{Lu}^{3+}$ -,  $\text{Yb}^{3+}$  and  $\text{Tm}^{3+}$ - solutions in  $0.20 \text{ mol}\cdot\text{L}^{-1}$   $\text{HCl}$  and with  $14 \text{ mol}\cdot\text{L}^{-1}$   $\text{LiCl}$  are worthwhile to consider. It could be shown that in solutions with low chloride concentrations, the Ln–O bond distance for  $\text{Yb}^{3+}$  is consistent with the fully hydrated  $\text{Yb}^{3+}$ . In solutions with an excess of  $\text{LiCl}$ , it was demonstrated that inner sphere chloro-complexation takes place together with a loss of water [34]. Furthermore, a current study in the terahertz frequency range of  $\text{YbCl}_3$  solutions using FT-IR spectroscopy [35] confirmed weak contact ion pairs as do our recent Raman results on  $\text{LuCl}_3(\text{aq})$  [17]. Choppin and Unrein [36] claimed that only outer-sphere ions pairs exist in lanthanide chloride solutions, but such a view has been questioned [17,29–32].

To summarize, the  $[\text{Yb}(\text{OH}_2)_7\text{Cl}]^{2+}$  modes in chloride solutions could be detected and formation of weak chloro-complexes with  $\text{Yb}^{3+}$  verified. In dilute solutions ( $C_T < 0.4 \text{ mol}\cdot\text{L}^{-1}$ ) the chloro-complex species disappeared upon dilution and  $[\text{Yb}(\text{OH}_2)_8]^{3+}$  and  $\text{Cl}^- (\text{aq})$  formed. The chloro-complex formation may be one reason for the data scatter of the recently published Yb–O bond distances and coordination numbers presented for  $\text{Yb}^{3+}(\text{aq})$  and other rare earth chloride systems [35,36]. In recent experimental structural studies, it was observed that inner-sphere chloro-complex species are formed

in aqueous  $\text{LnCl}_3$  solution ( $\text{Ln} = \text{Lu}$  and  $\text{Yb}$ ) with high chloride concentrations while in dilute solutions, fully hydrated ions exist [17,34,35].

#### 4. Conclusions

Raman measurements on dilute aqueous  $\text{Lu}(\text{ClO}_4)_3$ ,  $\text{Yb}(\text{ClO}_4)_3$ ,  $\text{Tm}(\text{ClO}_4)_3$ ,  $\text{Er}(\text{ClO}_4)_3$  and  $[\text{Ho}(\text{H}_2\text{O})_8]^{3+}$  solutions have been carried out. In these solutions, strongly polarized modes at  $396\text{ cm}^{-1}$ ,  $394\text{ cm}^{-1}$ ,  $391\text{ cm}^{-1}$ ,  $389\text{ cm}^{-1}$  and  $387\text{ cm}^{-1}$  were detected and assigned to the breathing modes,  $\nu_1 \text{Ln-O}$  of the octahydrates  $[\text{Lu}(\text{H}_2\text{O})_8]^{3+}$ ,  $[\text{Yb}(\text{H}_2\text{O})_8]^{3+}$ ,  $[\text{Tm}(\text{H}_2\text{O})_8]^{3+}$ ,  $[\text{Er}(\text{H}_2\text{O})_8]^{3+}$  and  $[\text{Ho}(\text{H}_2\text{O})_8]^{3+}$ , respectively. The force constants of these  $\text{Ln-O}$  breathing modes were calculated from these vibrational bands. In dilute perchlorate solutions, these species represent the fully hydrated  $[\text{Ln}(\text{OH}_2)_8]^{3+}$  ions. The calculated force constants of the octahydrates of  $[\text{Lu}(\text{H}_2\text{O})_8]^{3+}$ ,  $[\text{Yb}(\text{H}_2\text{O})_8]^{3+}$ ,  $[\text{Tm}(\text{H}_2\text{O})_8]^{3+}$ ,  $[\text{Er}(\text{H}_2\text{O})_8]^{3+}$  and  $[\text{Ho}(\text{H}_2\text{O})_8]^{3+}$  strengthen with the corresponding decrease of their  $\text{Ln-O}$  bond distances. The  $\text{Ln-O}$  bond of the five octahydrates is not very polarizable and therefore the scattering intensities of the  $\nu_1 \text{Ln-O}$  bands are small. In  $\text{Yb}(\text{ClO}_4)_3$  in heavy water, the  $\text{Yb-O}$  breathing mode shifts to  $375\text{ cm}^{-1}$  for the deuterated species  $[\text{Yb}(\text{OD}_2)_8]^{3+}$  as the result of the vibrational isotope effect changing from  $\text{H}_2\text{O}$  to  $\text{D}_2\text{O}$ .

As a representative example for the lanthanide perchlorate solutions, higher concentrated aqueous  $\text{Yb}(\text{ClO}_4)_3$  solutions were studied and in solutions  $> 2\text{ mol}\cdot\text{L}^{-1}$  a small fraction of contact ion pairs between  $\text{Yb}^{3+}$  and  $\text{ClO}_4^-$  were detected. This is supported by the parameters of  $\text{ClO}_4^-$ -bands (peak position, half width, band shapes) as well as changes of the band parameters of the  $\nu_1 \text{Yb-O}$  breathing mode.

In  $\text{YbCl}_3$  solutions,  $\text{Cl}^-$  penetrates into the first hydration sphere of  $\text{Yb}^{3+}(\text{aq})$  by pushing out a water molecule, and a weak 1:1 chloro-complex species forms. However, the fraction of the chloro-complex diminishes rapidly upon dilution and at a concentration  $< 0.4\text{ mol}\cdot\text{L}^{-1}$ , the chloro-complex species vanished. Our Raman spectroscopic findings were substantiated by recently published EXAFS and terahertz FT-IR and results [34,35].

**Supplementary Materials:** The following are available online. Table S1. Band fit data on of the anisotropic spectrum of an aqueous  $2.423\text{ mol}\cdot\text{L}^{-1}$   $\text{Yb}(\text{ClO}_4)_3$  solution in the terahertz region. Five  $\text{YbO}_8$  skeleton modes of  $[\text{Yb}(\text{H}_2\text{O})_8]^{3+}(\text{aq})$  were detected. In addition to isotropic band at  $390\text{ cm}^{-1}$  (fwhh =  $59\text{ cm}^{-1}$ ) was observed with an integrated band intensity = 3160. Figure S1. Raman scattering profiles ( $I_{VV}$  (black),  $I_{VH}$  (blue) and  $I_{iso}$  (red)) of a  $3.800\text{ mol}\cdot\text{L}^{-1}$   $\text{NaClO}_4(\text{aq})$  solution. The depolarized modes,  $\nu_2(e)$  at  $461\text{ cm}^{-1}$  and  $\nu_2(f_2)$  at  $629\text{ cm}^{-1}$  are the deformation modes of perchlorate,  $\text{ClO}_4^-$  (aq). The strongly polarized mode,  $\nu_1(a_1)$  at  $933\text{ cm}^{-1}$  is the  $\text{Cl-O}$  symmetric stretching mode and the depolarized band,  $\nu_3(f_2)$  at  $1110\text{ cm}^{-1}$  is due to the antisymmetric stretching mode of  $\text{ClO}_4^-$  (aq). The broad mode at  $1634\text{ cm}^{-1}$  is due to the deformation mode of  $\text{H}_2\text{O}$ . Figure S2. Top panel: Raman scattering profiles ( $R_{VV}$ ,  $R_{VH}$  and  $R_{iso}$ ) of a  $2.423\text{ mol}\cdot\text{L}^{-1}$   $\text{Yb}(\text{ClO}_4)_3$  solutions in water. The left inset shows the symmetric  $\text{YbO}_8$  stretching mode of  $[\text{Yb}(\text{H}_2\text{O})_8]^{3+}$  at  $390\text{ cm}^{-1}$ . Note the perchlorate bands at  $461\text{ cm}^{-1}$  and at  $629\text{ cm}^{-1}$  as well as the band at  $1112\text{ cm}^{-1}$ . The inset at the right shows the  $\nu_1\text{ClO}_4^-$  mode at its full scale. Shown are the isotropic scattering profile (red), the anisotropic one (blue) and the polarized scattering (black). Bottom panel: Raman spectrum of the  $2.423\text{ mol}\cdot\text{L}^{-1}$   $\text{Yb}(\text{ClO}_4)_3$  solution in the wavenumber region from  $1400\text{ cm}^{-1}$  to  $4160\text{ cm}^{-1}$  (spectra in I-format: from top to bottom: polarized (black), depolarized (blue) and isotropic (red) scattering profiles). The deformation mode of water appears at  $1623\text{ cm}^{-1}$  and in the O-H stretching region the water band is modified by the typical  $\text{ClO}_4^- \text{H}_2\text{O}$  mode of weakly hydrogen bonded O-H oscillators. The band at  $3538 \pm 3\text{ cm}^{-1}$  is due to the stretching bands of the weakly bonded O-H... $\text{OCLO}_3^-$  units of  $\text{H}_2\text{O}/\text{ClO}_4^-$ . Figure S3. Integrated band intensity,  $A_{394}$ , of the symmetric stretching mode  $\nu_1\text{YbO}_8$  in arbitrary units as a function of the  $\text{Yb}(\text{ClO}_4)_3$  solution concentration. Figure S4. Isotropic Raman scattering profile (R-format) of a  $1.25\text{ mol}\cdot\text{L}^{-1}$   $\text{Yb}(\text{CF}_3\text{SO}_3)_3$  solution. In addition to the strong triflate band at  $319.5\text{ cm}^{-1}$  a very weak and relatively broad band appears at  $394\text{ cm}^{-1}$  which is assigned to the totally symmetric stretching mode of  $\text{YbO}_8$ . Figure S5. Raman scattering profiles of a  $1.276\text{ mol}\cdot\text{L}^{-1}$   $\text{Yb}(\text{ClO}_4)_3$  solution in heavy water in order to observe the isotope effect on the symmetric stretching mode of the hydrate respectively deuterated species by changing from  $[\text{Yb}(\text{H}_2\text{O})_8]^{3+}(\text{H}_2\text{O})$  to  $[\text{Yb}(\text{D}_2\text{O})_8]^{3+}(\text{D}_2\text{O})$ . Shown are the isotropic scattering profile (red), the anisotropic one (blue) and the polarized scattering (black). Figure S6.  $\text{Tm}(\text{ClO}_4)_3$  solution at  $0.315\text{ mol}\cdot\text{L}^{-1}$  ( $R_w = 226.6$ ) in R-format (spectra from top to bottom:  $R_{VV}$ ,  $R_{VH}$  and  $R_{iso}$ ). The inset shows the  $R_{iso}$  spectrum in greater detail. Note the broad and weak  $\nu_1\text{TmO}_8$  stretching mode at  $391\text{ cm}^{-1}$  (fwhh =  $53\text{ cm}^{-1}$ ) of the  $[\text{Tm}(\text{OH}_2)_8]^{3+}$  species. The much larger, depolarized

bands at  $461\text{ cm}^{-1}$  and  $629\text{ cm}^{-1}$  are the deformation modes of perchlorate,  $\text{ClO}_4^-$  (aq). Shown are the isotropic scattering profile (red), the anisotropic one (blue) and the polarized scattering (black). Figure S7. Polarized Raman scattering profile of an aqueous  $\text{Er}(\text{ClO}_4)_3$  solution at  $0.321\text{ mol}\cdot\text{L}^{-1}$ . The weak and strongly polarized mode at  $389\text{ cm}^{-1}$  is assigned to the Er-O symmetric stretching mode of  $[\text{Er}(\text{OH}_2)_8]^{3+}$ . Note the strong deformation mode,  $\nu_2(\text{e})\text{ ClO}_4^-$  (aq) at  $461\text{ cm}^{-1}$ . Figure S8. Polarized Raman scattering profile of an aqueous  $\text{Ho}(\text{ClO}_4)_3$  solution at  $0.240\text{ mol}\cdot\text{L}^{-1}$ . The weak and strongly polarized mode at  $387\text{ cm}^{-1}$  is assigned to the Ho-O symmetric stretching mode of  $[\text{Ho}(\text{OH}_2)_8]^{3+}$ . Note the strong deformation mode,  $\nu_2(\text{e})\text{ ClO}_4^-$  (aq) at  $461\text{ cm}^{-1}$ . Figure S9. The heavy REE ions at the X-axis from left to right:  $\text{Ho}^{3+}$ ,  $\text{Er}^{3+}$ ,  $\text{Tm}^{3+}$ ,  $\text{Yb}^{3+}$ , and  $\text{Lu}^{3+}$ . At the left Y-axis the peak positions of the corresponding breathing modes,  $\nu_1\text{ Ln-O}$  are given and at the right Y-axis the Ln-O bond distances of the octahydrates,  $[\text{Ln}(\text{OH}_2)_8]^{3+}$  [7]. Figure S10. Raman scattering profiles in R-format ( $R_{\text{VV}}$  (black),  $R_{\text{VH}}$  (blue) and  $R_{\text{iso}}$  (red) scattering) of a  $0.422\text{ mol}\cdot\text{L}^{-1}$   $\text{YbCl}_3$  solutions in heavy water. The  $\text{YbO}_8$  symmetric stretch of  $[\text{Yb}(\text{D}_2\text{O})_8]^{3+}(\text{D}_2\text{O})$  ( $\text{D}_2\text{O}$  taken as point mass) is shifted to  $376\text{ cm}^{-1}$  while the same mode in light water is observed at  $394\text{ cm}^{-1}$  demonstrating the vibrational isotope effect on the symmetric stretching mode by changing from  $[\text{Yb}(\text{H}_2\text{O})_8]^{3+}(\text{aq})$  to  $[\text{Yb}(\text{D}_2\text{O})_8]^{3+}(\text{D}_2\text{O})$ . Note furthermore the restricted translation band of the O-D...D unit at  $182\text{ cm}^{-1}$ , the librational band at  $547\text{ cm}^{-1}$  and the deformation mode  $\nu_2\text{ D-O-D}$  at  $1205\text{ cm}^{-1}$ . The mode at  $1445\text{ cm}^{-1}$  stems from the small amount of HDO and the band at  $1542\text{ cm}^{-1}$  is a combination band of  $\text{D}_2\text{O}$ . Figure S11. The linear dependence of the integrated band intensity,  $A_{394}$  as a function of the  $\text{Yb}(\text{ClO}_4)_3$  concentration with  $A_{394} = 1303.7 \times C_{\text{T}}$  (see Figure S4). The lower curve shows the integrated band intensity of the band at  $394\text{ cm}^{-1}$  in  $\text{YbCl}_3$  solutions (black squares). The solute concentration is denoted as  $C_{\text{T}}$ .

**Author Contributions:** Conceptualization, W.R. and G.I.; methodology, W.R.; software, G.I.; validation, W.R., G.I.; formal analysis, W.R.; investigation, W.R.; resources, W.R.; data curation, W.R.; writing—original draft preparation, W.R.; writing—review and editing, W.R.; visualization, W.R.; supervision, W.R.; project administration, W.R.; funding acquisition, W.R.

**Funding:** This research received no external funding.

**Acknowledgments:** We thank J. Kortus of the Institut für Theoretische Physik, TU Bergakademie Freiberg, Germany for his hospitality and permission for the use of the Raman spectrometer. We are grateful to the colleagues of the Institut for their hospitality and stimulating discussions. We particularly wish to acknowledge Frau B. Ostermay for her help in measuring the samples.

**Conflicts of Interest:** The authors declare no conflict of interest.

## References

1. Huang, C.H.; Bian, Z. *Introduction in Rare Earth Coordination Chemistry: Fundamentals and Applications*; Huang, C.-H., Ed.; Wiley: New York, NY, USA, 2010.
2. Marcus, Y. A simple empirical model describing the thermodynamics of hydration of ions of widely varying charges, sizes, and shapes. *Biophys. Chem.* **1994**, *51*, 111–127. [[CrossRef](#)]
3. Burgess, J. *Ions in Solution: Basic Principles of Chemical Interactions*; Ellis Horwood, Chichester/Halsted Press: New York, NY, USA, 1988.
4. Habenschuss, A.; Spedding, F.H. The coordination (hydration) of rare earth ions in aqueous chloride solutions from x ray diffraction. I.  $\text{TbCl}_3$ ,  $\text{DyCl}_3$ ,  $\text{ErCl}_3$ ,  $\text{TmCl}_3$ , and  $\text{LuCl}_3$ . *J. Chem. Phys.* **1979**, *70*, 2797–2806. [[CrossRef](#)]
5. Cossy, C.; Barnes, A.C.; Enderby, J.E.; Merbach, A.E. The hydration of dysprosium(3+) and ytterbium(3+) in aqueous solution: A neutron scattering first order difference study. *J. Chem. Phys.* **1989**, *90*, 3254–3260. [[CrossRef](#)]
6. Cossy, C.; Helm, L.; Powell, D.H.; Merbach, A.E. A change in coordination number from nine to eight along the lanthanide(III) aqua ion series in solution: A neutron diffraction study. *New J. Chem.* **1995**, *19*, 27–35.
7. Persson, I.; D'Angelo, P.; Panifilis, S.D.; Sandström, M.; Eriksson, L. Hydration of Lanthanoid(III) Ions in Aqueous Solution and Crystalline Hydrates Studied by EXAFS Spectroscopy and Crystallography: The Myth of the “Gadolinium Break”. *Chem.-Eur. J.* **2008**, *14*, 3056–3066. [[CrossRef](#)] [[PubMed](#)]
8. Spezia, R.; Duvail, M.; Vitorge, P.; D'Angelo, P. Molecular dynamics to rationalize EXAFS experiments: A dynamical model explaining hydration behaviour across the lanthanoid(III) series. *J. Phys. Conf. Ser.* **2009**, *190*, 012056. [[CrossRef](#)]
9. Sessa, F.; Spezia, R.; D'Angelo, P. Lutetium(III) aqua ion: On the dynamical structure of the heaviest lanthanoid hydration complex. *J. Chem. Phys.* **2016**, *144*, 204505. [[CrossRef](#)]
10. D'Angelo, P.; Spezia, R. Hydration of Lanthanoids(III) and Actinoids(III): An Experimental/Theoretical Saga. *Chem. Eur. J.* **2012**, *18*, 11162–11178. [[CrossRef](#)] [[PubMed](#)]



11. Duvail, M.; D'Angelo, P.; Gaigeot, M.P.; Vitorge, P.; Spezia, R. What first principles molecular dynamics can tell us about EXAFS spectroscopy of radioactive heavy metal cations in water. *Radiochim. Acta* **2009**, *97*, 339–346. [[CrossRef](#)]
12. Duvail, M.; Spezia, R.; Vitorge, P.A. Dynamic Model to Explain Hydration Behaviour along the Lanthanide Series. *Chem. Phys. Chem.* **2008**, *9*, 693–696. [[CrossRef](#)] [[PubMed](#)]
13. Passler, P.P.; Rode, B.M. Thulium(III) and ytterbium(III) in aqueous solution ab initio quantum mechanical charge field molecular dynamics studies. *Chem. Phys. Lett.* **2015**, *638*, 128–132. [[CrossRef](#)]
14. Rudolph, W.W.; Irmer, G. Hydration and ion pair formation in common aqueous La(III) salt solutions—A Raman scattering and DFT study. *Dalton Trans* **2015**, *44*, 295–305. [[CrossRef](#)] [[PubMed](#)]
15. Rudolph, W.W.; Irmer, G. Raman spectroscopic characterization of light rare earth ions: La<sup>3+</sup>, Ce<sup>3+</sup>, Pr<sup>3+</sup>, Nd<sup>3+</sup> and Sm<sup>3+</sup>—hydration and ion pair formation. *Dalton Trans.* **2017**, *46*, 4235–4244. [[CrossRef](#)]
16. Rudolph, W.W.; Irmer, G. Hydration and ion pair formation in aqueous Y<sup>3+</sup>—salt solutions. *Dalton Trans.* **2015**, *44*, 18492–18505. [[CrossRef](#)] [[PubMed](#)]
17. Rudolph, W.W.; Irmer, G. Hydration and ion pair formation in aqueous Lu<sup>3+</sup> - solution. *Molecules* **2018**, *23*, 3237. [[CrossRef](#)]
18. Schwarzenbach, G.; Flaschka, H.A. *Die Komplextometrische Titration*; F. Enke Verlag: Stuttgart, Germany, 1965.
19. Rudolph, W.W.; Irmer, G. Raman and Infrared Spectroscopic Investigations on Aqueous Alkali Metal Phosphate Solutions and Density Functional Theory Calculations of Phosphate—Water Clusters. *Appl. Spectrosc.* **2007**, *61*, 1312–1327. [[CrossRef](#)]
20. Rudolph, W.W.; Brooker, M.H.; Pye, C.C. Hydration of Lithium Ion in Aqueous Solutions. *J. Phys. Chem.* **1995**, *99*, 3793–3797. [[CrossRef](#)]
21. LaPlant, F.; Laurence, G.; Ben-Amotz, D. Theoretical and Experimental Uncertainty in Temperature Measurement of Materials by Raman Spectroscopy. *Appl. Spectrosc.* **1996**, *50*, 1034–1038. [[CrossRef](#)]
22. Rudolph, W.W.; Mason, R.; Pye, C.C. Aluminium(III) hydration in aqueous solution. A Raman spectroscopic investigation and an ab initio molecular orbital study of aluminium(III) water clusters. *Phys. Chem. Chem. Phys.* **2000**, *2*, 5030–5040. [[CrossRef](#)]
23. Rudolph, W.; Schönherr, S. Raman-und Infrarotspektroskopische Untersuchungen an konzentrierten Aluminiumsalzlösungen. *Z. Phys. Chem.* **1989**, *270*, 1121–1134.
24. Cossy, C.; Helm, L.; Merbach, A.E. Oxygen-17 Nuclear Magnetic Resonance Kinetic Study of Water Exchange on the Lanthanide(III) Aqua Ions. *Inorg. Chem.* **1988**, *27*, 1973–1979. [[CrossRef](#)]
25. Pearson, R.G. Hard and Soft Acids and Bases. *J. Am. Chem. Soc.* **1963**, *85*, 3533–3539. [[CrossRef](#)]
26. Kanno, H. Hydrations of metal ions in aqueous electrolyte solutions: A Raman study. *J. Phys. Chem.* **1988**, *92*, 4232–4236. [[CrossRef](#)]
27. Helm, L.; Merbach, A.E. Applications of advanced experimental techniques: High pressure NMR and computer simulations. *J. Chem. Soc. Dalton Trans.* **2002**, *5*, 633–641. [[CrossRef](#)]
28. Purdie, N.; Farrow, M.M. The application of ultrasound-absorption to reaction kinetics. *Coord. Chem. Rev.* **1973**, *11*, 189–226. [[CrossRef](#)]
29. Wood, S.A. The aqueous geochemistry of the rare-earth elements and yttrium. 1. Review of available low-temperature data for inorganic complexes and the inorganic REE speciation of natural waters. *Chem. Geol.* **1990**, *82*, 159–186. [[CrossRef](#)]
30. Fernández-Ramírez, E.; Jiménez-Reyes, M.; Solache-Ríos, M.J. Effects of Ionic Strength and Charge Density on the Stability of Chloride Complexes of Trivalent Lanthanides. *J. Chem. Eng. Data* **2008**, *53*, 1756–1761. [[CrossRef](#)]
31. Fukasawa, T.; Kawasuji, I.; Mitsugahiro, T.; Sat, A.; Suzuki, S. Investigation on the Complex Formation of Some Lanthanoids(III) and Actinoids(III) with chloride and Bromide. *Bull. Chem. Soc. Jpn.* **1982**, *55*, 726–729. [[CrossRef](#)]
32. Marcus, Y. Anion exchange of metal complexes—XV: Anion exchange and amine extraction of lanthanides and trivalent actinides from chloride solutions. *J. Inorg. Nucl. Chem.* **1966**, *28*, 209–219. [[CrossRef](#)]
33. Pye, C.C.; Corbeil, C.R.; Rudolph, W.W. An ab initio investigation of zinc chloro complexes. *Phys. Chem. Chem. Phys.* **2006**, *8*, 5428–5436. [[CrossRef](#)] [[PubMed](#)]
34. Allen, P.G.; Bucher, J.J.; Shuh, D.K.; Edelstein, N.M.; Craig, I. Coordination chemistry of trivalent lanthanide and actinide ions in dilute and concentrated chloride solutions. *Inorg. Chem.* **2000**, *39*, 595–601. [[CrossRef](#)] [[PubMed](#)]

35. Klinkhammer, C.; Böhm, F.; Sharma, V.; Schwaab, G.; Seitz, M.; Havenith, M. Anion dependent ion pairing in concentrated ytterbium halide solutions. *J. Chem. Phys.* **2018**, *148*, 222802. [[CrossRef](#)] [[PubMed](#)]
36. Choppin, G.R.; Unrein, P.J. Halide complexes of the lanthanide elements. *J. Inorg. Nucl. Chem.* **1963**, *25*, 387–393. [[CrossRef](#)]

**Sample Availability:** Samples of the Ytterbium salts are available from the authors.



© 2019 by the authors. Licensee MDPI, Basel, Switzerland. This article is an open access article distributed under the terms and conditions of the Creative Commons Attribution (CC BY) license (<http://creativecommons.org/licenses/by/4.0/>).